ARMY RESEARCH LABORATORY

An Overview of High-Explosive (HE) Blast Damage Mechanisms and Vulnerability Prediction Methods

by Abdul R. Kiwan

ARL-TR-1468 August 1997

The findings in this report are not to be construed as an official Department of the Army position unless so designated by other authorized documents.

Citation of manufacturer's or trade names does not constitute an official endorsement or approval of the use thereof.

Destroy this report when it is no longer needed. Do not return it to the originator.

Army Research Laboratory
Aberdeen Proving Ground, MD 21005-5068

ARL-TR-1468 **August 1997**

An Overview of High-Explosive (HE) Blast Damage Mechanisms and Vulnerability Prediction Methods

Abdul R. Kiwan
Survivability/Lethality Analysis Directorate, ARL

Abstract

An overview of high-explosive (HE) blast phenomenology, its models, methods, and the scaling of results are presented. Experimental data of HE blast damage to various types of structures are also presented, together with some of the HE blast structural damage models. Empirical vulnerability models of weapon systems to HE blast are also discussed.

Table of Contents

List of Figures

1. Introduction

To explain what is meant by the term "high-explosive (HE) blast damage mechanism," we first need to define the meaning we attach to the words "blast wave." A blast wave is a pressure wave generated in the air by the rapid release of energy stored in some source into the surrounding medium. There are many sources of stored energy that give rise to such pressure waves. The stored energy in a compressed gas or vapor, either hot or cold, can be such a source. The failure of a high-pressure gas storage vessel or boiler, or the muzzle blast from a gun, is an example of explosions that give rise to a blast wave in air. However, the more usual sources of energy for explosions and generation of blast waves are either chemical or nuclear materials that are capable of violent reactions when properly initiated. Here we shall confine our interest to blast waves generated by the detonation of HE charges (i.e., chemical energy sources).

In order to facilitate the study of HE blast waves, an explosive material is chosen as a reference material for all explosives, and the properties of blast waves from spherical or cylindrical charges of this reference explosive are documented and considered a standard explosive. Two explosives have been used as such a standard, TNT and Pentolite, and their properties have been studied and documented. The blast properties of all other explosives are usually derived by some equivalency to one of the standard explosives. The blast properties of TNT were documented by Swisdak [1], mostly for use in U.S. Navy (USN) publications. The detonation and blast properties of Pentolite were studied by many researchers and documented by Goodman [2] for the U.S. Army Ballistic Research Laboratory (BRL). Pentolite is widely used as a standard explosive because of its more reproducible properties. The detonation and blast properties of 24 selected explosives were calculated by Shear and Arbuckle [3]. Many other publications exist on the subject, in particular, the U.S. Army Materiel Command (AMC) explosive series, "Properties of Explosives of Military Interest" [4]. Next, we describe in more detail what is meant by the term "blast wave."

When energy from a source is rapidly released into the surrounding medium, a finite pressure wave of compressible gas propagates through the medium. The front of the disturbance

steepens as it propagates forward. The air is said to be shocked up as it passes through the front, and the wave is termed to be a "shock wave." The shock wave front propagates at supersonic speed as it travels through the undisturbed air. The shock wave front constitutes a jump discontinuity in the properties of the air behind the front. The term "blast wave" will be taken to mean a shock wave generated by the detonation of an HE charge in the ambient air or by one of the energy sources previously mentioned. The interest in our present study is confined to blast waves generated by the detonation of HE charges.

2. Description of a Generic Blast Wave

2.1 Blast Wave in Free Air. Let us consider the characteristics of an ideal blast wave formed in the air by some energy source. Assume that an HE explosion occurred in air, that it is spherically symmetric, and that the atmosphere is homogeneous. It follows that the characteristics of the air behind the shock front are only functions of the distance R from the source of the disturbance and the elapsed time t. If an ideal pressure transducer that offers no resistance to the flow behind the shock front was located a short distance from the source of the HE explosion, then this transducer will record the variations of the pressure behind the shock wave as it sweeps over the transducer. The record produced by such a transducer will resemble that shown in Figure 1. For some time after the explosion, the transducer records ambient pressure p_0 until the shock wave arrival. At arrival time t_a, the pressure rises quite abruptly (discontinuously in an ideal wave) to a peak value $p_0 + p_s^+$. The pressure then decays to ambient in a total time $t_a + T^+$, drops to a partial vacuum of amplitude p_s^-, and eventually returns to p_0 in total time $t_a + T^+ + T^-$. The quantity p_s^+ is usually termed the peak side-on overpressure or merely the peak overpressure. The portion of the time history above the initial ambient pressure p_0 is called the positive phase of duration T^+. The portion below p_0, of amplitude p_s^- and duration T^-, is called the negative phase. The positive and negative impulses defined by the equations

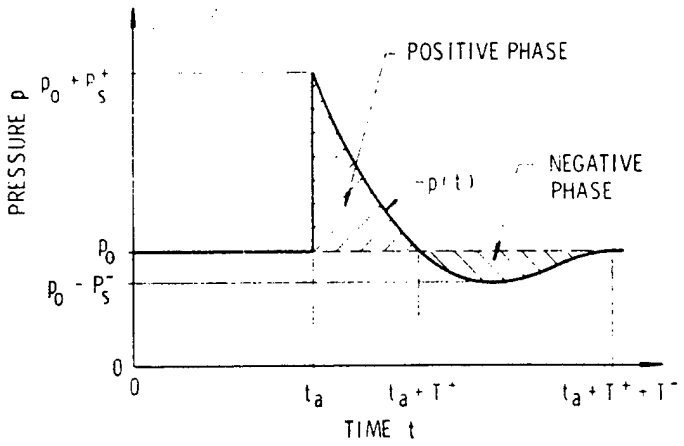

Figure 1. Ideal Blast Wave.

$$I_s^+ = \int_{t_a}^{t_a + T^+} [p(t) - p_0]\, dt \tag{1}$$

and

$$I_s^- = \int_{t_a + T^+}^{t_a + T^+ + T^-} [p_0 - p(t)]\, dt \tag{2}$$

are important blast wave parameters. In the following, we shall focus our attention only on the characteristics of the positive phase part of the blast wave and its significant parameters. Henceforth, any blast wave parameters mentioned will refer only to the positive phase part only. In order to describe the characteristics of an ideal blast wave, we first need a functional description of its pressure-time history. Several functional forms have been proposed for that purpose. A two-parameter form approximates the wave with a straight line that preserves two of the blast wave parameters (e.g., p_s^+ and T^+), as is the case in equation (3):

$$p(t) = p_0 + P_s^+ (1 - t/T^+),\ 0 < t <= T^+, \tag{3}$$

where, t_a is assumed to be zero and henceforth. A frequently used three-parameter form is the "modified Friedlander equation":

$$p(t) = p_0 + P_s^+ (1 - t/T^+) e^{-bt/T^+},\ 0 < t <= T^+. \tag{4}$$

This three-parameter form allows one to match any three of the four blast characteristic parameters, P_s^+, T^+, I_s^+, and initial decay rate dp/dt(t = 0). A more complex four-parameter form has been proposed by Ethridge [5] that will match all the blast parameters previously shown. Excellent references on the phenomenology of blast waves and explosions can be found in AMCP 706-181 [6] or Baker [7].

2.2 Shock Wave Reflection. When a shock wave strikes a rigid wall or a solid obstacle, the properties of the wave are changed considerably as the wave reflects from the obstacle or diffracts around it. Many books exist that discuss the subjects of wave reflection or diffraction in detail. For our purposes, we shall briefly describe the phenomenon of normal reflection of a plane shock wave and make a few general comments about shock wave reflections. Figure 2 illustrates schematically the reflection of a plane incident wave I from a rigid wall. The shock front moves at a velocity U into the ambient atmosphere with properties p_0, ρ_0, θ_0, and $u_0 = 0$ denoting the pressure, density, temperature, and particle velocity. The flow behind the shock front is characterized by the pressure, density, temperature, and particle velocity denoted by $p_0 + P_s$, ρ_s, θ_s, and u_s. At the rigid wall, the particle velocity is reduced to zero, $u_r = 0$. The reflected wave front R moves away from the wall at a velocity U_r into the flow field behind the incident wave. The overpressure, density, and temperature behind the reflected wave are substantially increased to new values, $p_0 + P_r$, ρ_r, and θ_r. For a weak shock wave (i.e., $P_s << p_0$), the reflected overpressure can be shown to be $P_r = 2\,P_s$, and the wave is called an acoustic wave. In general, the reflected overpressure can be many times the incident overpressure. For an ideal gas, it can be shown that $P_r = 8 \cdot P_s$. However, it was shown by Doering and Burkhardt [8] and Shear and McCane [9] that air does not behave as an ideal gas under high-temperature and high-pressure conditions. It is believed that under such conditions, P_r can be as large as $20 \cdot P_s$. Shock waves can also reflect obliquely from a solid obstacle or rigid wall. This reflection phenomenon, as well as the Mach reflection of a shock wave, are highly complex and are beyond the scope of this study. The interested reader should see Baker [7] and Courant and Friedrichs [10].

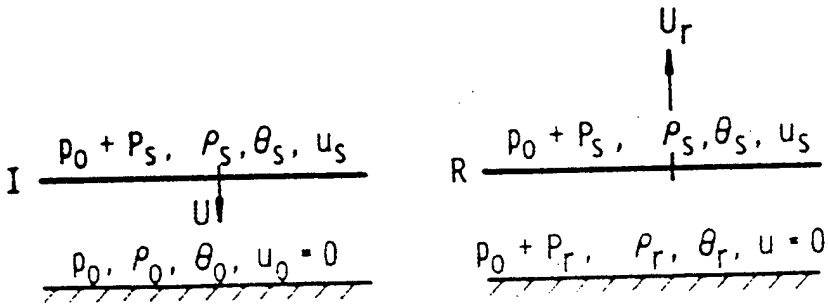

Figure 2. Normal Reflection of a Plane Shock Wave From a Rigid Wall.

2.3 Blast Parameters Scaling Laws. Determination of the blast parameters that characterize the blast wave from an explosive charge W detonated in the air can be made by experimental means. These experiments are costly and time consuming. Computational methods for calculating blast wave parameters are also highly complex, time consuming, and expensive. Early on, researchers started looking for scaling methods in order to derive from their experiments the values of blast parameters for many more similar explosive charges of different size without resorting to experiments for each possible variation of characteristic parameters. Hopkinson or "cube root" scaling is most widely used by people who deal with blast waves from explosive charges. This scaling law states that self-similar blast (shock) waves are produced in air when two explosive charges of the same geometry and composition but of different sizes are detonated. Symbolically stated as:

$$p = p(Z),\ \tau = \tau(Z),\ U = U(Z),\ \zeta = \zeta(Z) \tag{5}$$

where,

$$Z = R/E^{1/3},\ \tau = \tau/E^{1/3},\ \text{and}\ \zeta = I/E^{1/3}. \tag{6}$$

p, I, U, and E denote the pressure, impulse, velocity, and total energy. R is the radial distance measured from the center of the charge, and t denotes the time. Z, τ, and ζ are designated scaled distance, scaled time, and scaled impulse. Hopkinson scaling has been verified experimentally over a wide range of scaled distances and can also be derived from dimensional analysis considerations [6]. Traditionally, experimentalists have used (instead of the dimensionless scaled variables of Z, τ, and ζ defined previously) dimensional scaled variables that result from the previous definition by replacing the variable E by W, the charge weight in those definitions. Since W is proportional to E, Hopkinson scaling still holds in this form that is most commonly used. This scaling states that pressures and velocities are identical at the same scaled distances Z, and similarly scaled impulse and time are functions of Z only. This scaling law is commonly used to predict the blast parameters for spherical HE charges from the documented properties of Pentolite by Goodman [2] or from those of TNT as documented by Swisdak [1]. Peak shock overpressures, impulse, and time of positive durations can be predicted for the side-on free air values or for the normally reflected wave parameter values from established standard curves and tables. Hopkinson scaling is also used to predict blast parameter values for cylindrical HE charges from established data for such charges. Predictions of blast parameter values such as overpressure and impulse are essential for predicting the blast damage to the various structural components of a target subjected to HE blast.

In order to account for the variations in the values of the blast parameters with altitude conditions, Sachs [11] proposed a more general scaling law than Hopkinson's scaling. Sachs' scaling states that dimensionless parameters involving pressure, time, and impulse can be defined in combination with other parameters of the ambient atmosphere so that they are unique functions of a dimensionless distance parameter. Symbolically, it can be stated that the dimensionless parameters

$$p/p_0,\ I \cdot a_0/(E \cdot p_0^2)^{1/3},\ t \cdot a_0 \cdot p_0^{1/3}/E^{1/3} \tag{7}$$

are unique functions of the dimensionless scaled distance;

$$R \cdot p_0^{1/3}/E^{1/3}, \tag{8}$$

where p, I, R, and t represent the pressure, impulse, radial distance from the charge center, and the time. E is the total energy, with a_0 and p_0 being the sound speed and the ambient atmospheric pressure. Sperrazza [12] gave a derivation of Sachs scaling using dimensional analysis argument; Dewey and Sperrazza [13] verified the scaling experimentally. Using superscripts on variables to denote altitude values and zero subscripts to denote ambient atmosphere values of parameters, Sachs scaling can be stated by the following equations:

$$P^{(h)}/p_0^{(h)} = P^{(0)}/p_0^{(0)}, \tag{9}$$

$$a_0^{(h)} \cdot I^{(h)}/\left(E^{(h)} \cdot p_0^{(h)^2}\right)^{1/3} = a_0^{(0)} \cdot I^{(0)}/\left(E^{(0)} \cdot p_0^{(0)^2}\right)^{1/3}, \tag{10}$$

and

$$t^{(h)} \cdot a_0^{(h)} \cdot \{p_0^{(h)}/E^{(h)}\}^{1/3} = t^{(0)} \cdot a_0^{(0)} \cdot \{p_0^{(0)}/E^{(0)}\}^{1/3}. \tag{11}$$

Equations (9)–(11) summarize Sachs' scaling law. These equations, together with equation (8), can be used to predict values of the blast parameters at altitude condition (h) from values measured at sea level. Values of blast parameters at altitude conditions are essential for vulnerability/lethality studies of aircraft and missiles in flight.

3. Illustrative Experimental Test Results

• **HE Blast vs. Rolled Homogeneous Armor (RHA) Plates, Aluminum Plates, Cylinders, Trucks, Armored Personnel Carriers (APCs), Scaled Chemical Submunition Cylinders, and Aircraft.** Some experimental test data exist on the damage caused by HE blast waves to various structures. Data of HE blast damage to RHA plates of 3/16–3/4-in thickness have been documented in Kiwan and Goodman [14]. Figures 3, 4, and 5 show the various types of damage observed in these experiments. The data gathered in these tests consisted of measurements of deformation, reduction in thickness, failure threshold parameters values, and hole size

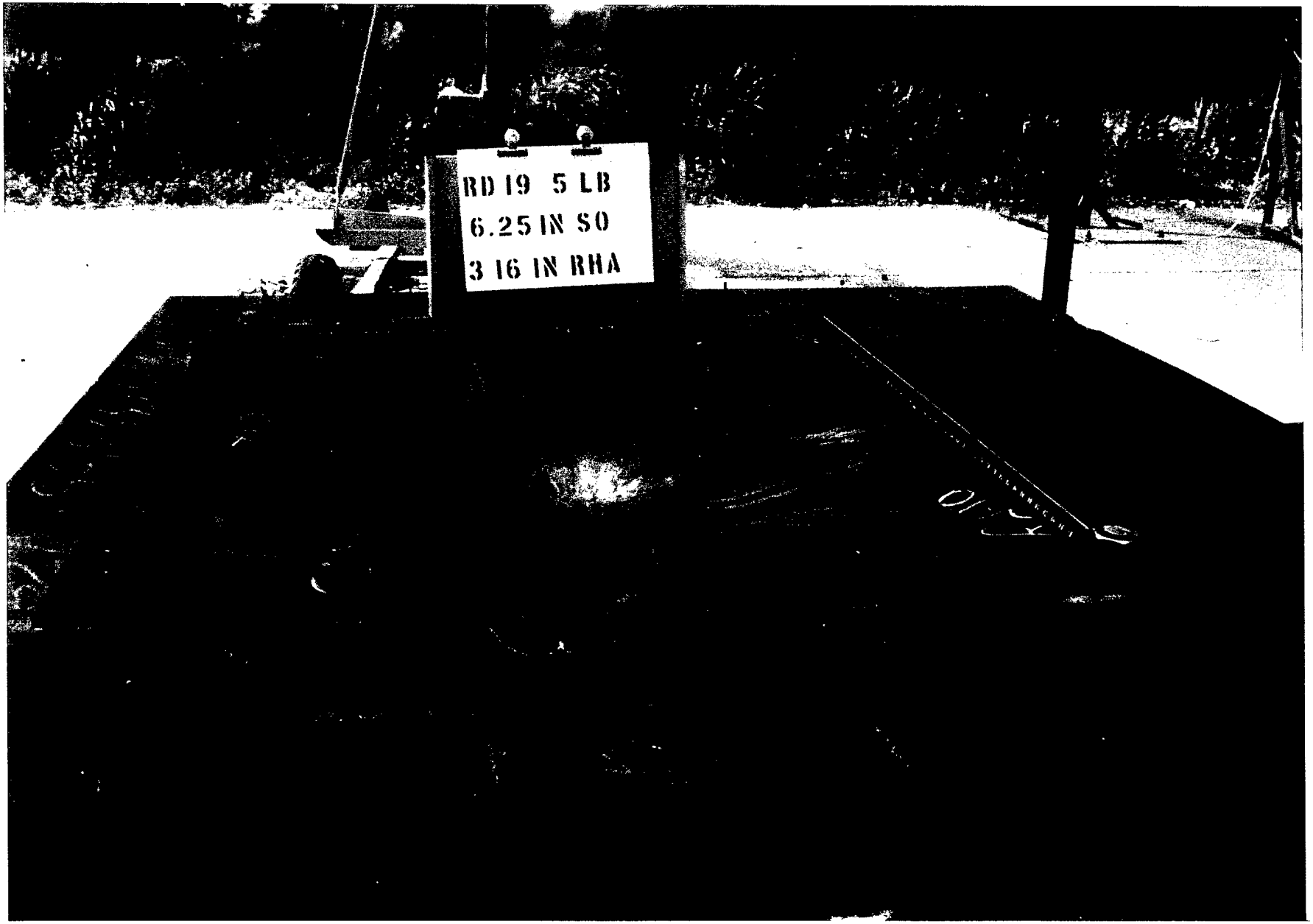

Figure 3. Damage to a 3/16-in-Thick RHA Plate by a 5-lb Spherical Pentolite Charge at a 6.25-in Standoff.

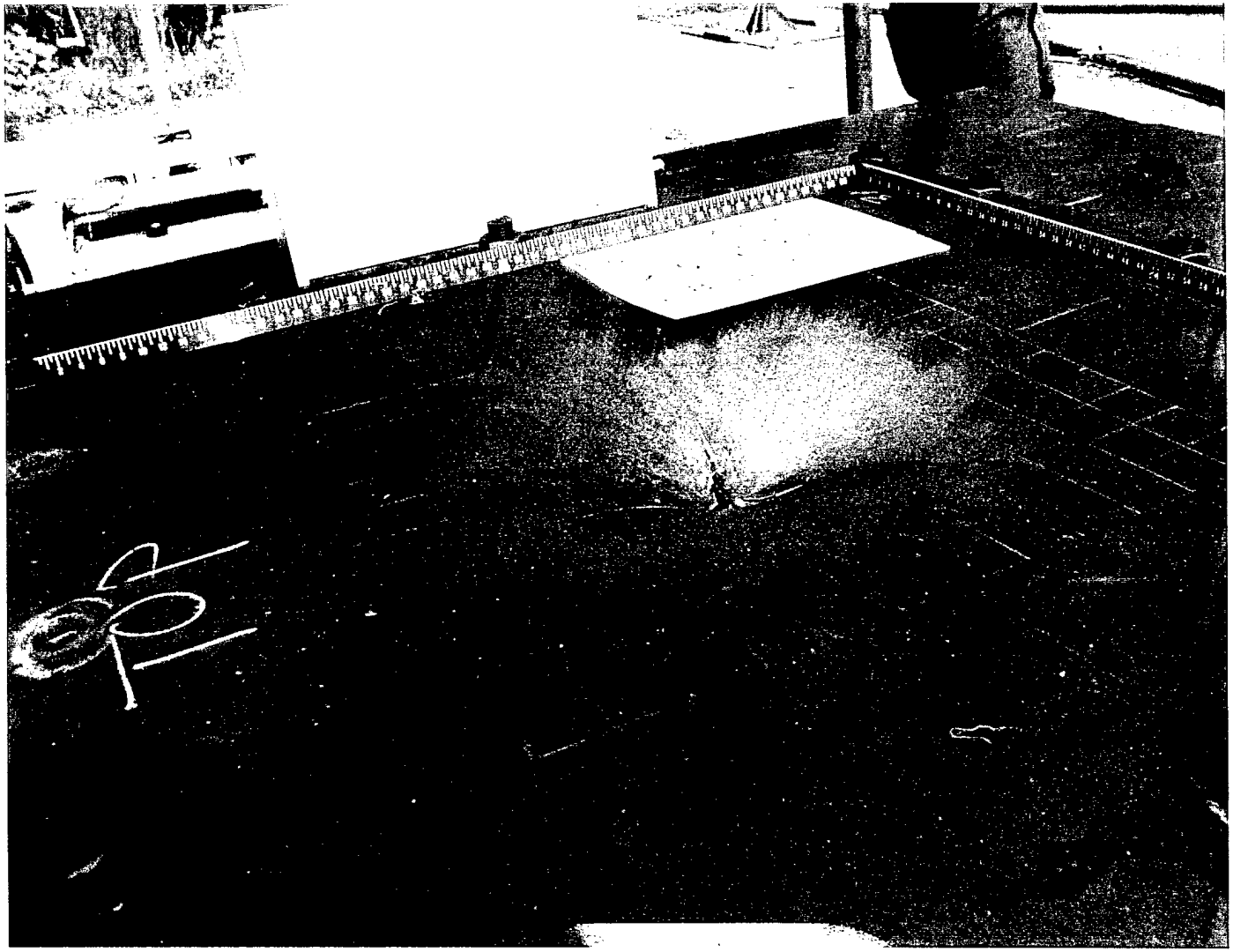

Figure 4. Damage to a 3/8-in-Thick RHA Plate by a 2-lb Spherical Pentolite Charge at a 2.5-in Standoff.

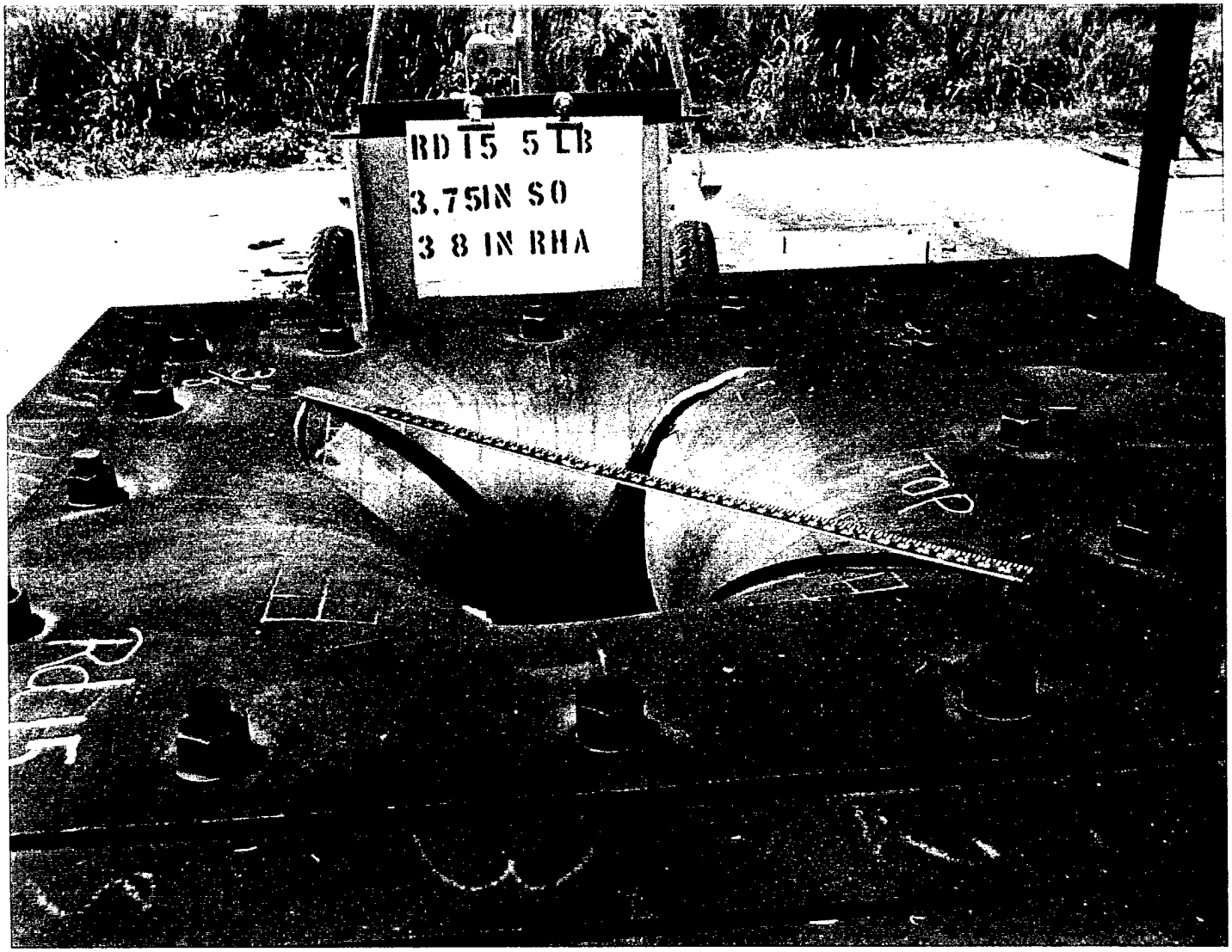

Figure 5. Damage to a 3/8-in-Thick RHA Plate by a 5-lb Spherical Pentolite Charge at a 3.75-in Standoff.

measurements. The experimental test data were used to construct a mathematical model for the response of armor to HE blast loading. The developed model will be discussed in section 4.2. Figure 3 shows the HE blast damage of an RHA plate 3/16 in thick from the detonation of a 5-lb Pentolite charge at a standoff of 6.25 in. The observed damage consisted of deformation and buckling. Figure 4 shows the more severe damage of material failure with three cracks propagating from the plate's center. Figure 5 shows a more severe type of damage of a hole opening up, with cracks propagating toward the plate's boundary and petaling.

Some experimental data exist on the response of aluminum 2024 plates to blast loading from 2-lb Pentolite charges. The available data are limited to plate thicknesses of 0.090 and 0.125 in. Figure 6 shows the blast damage from a 2-lb Pentolite charge detonated at a standoff of 11 9/16 in from an aluminum 2024 plate 0.090 in thick. The plate failed in shear along the entire clamped, supported boundary. Figure 7 shows a similar experiment but at a standoff of 22 in. Buckling and tearing were observed at the central bolts in addition to the deformation and the tearing at the corners. Figure 8 shows a similar test for a plate of 0.125-in thickness at a charge standoff of 13 in. The damage observed in these experiments differed in nature from the damage observed on the RHA plates. The aluminum 2024 deformed plastically but then failed in shear at the boundary starting at the plate's corners. The RHA plates failed in tension from the plate's center. Schuman [15, 16] conducted extensive experiments on the blast damage to aluminum and steel cylinders. The results of these experiments and research are documented in noted references. The resulting damage model of Schuman will be described briefly in section 4.3. Baker et al. [17] investigated the response of cantilever beams to air blast loading.

Experimental test data of the response of structures of various weapon systems to HE blast loading exist, although sometimes not in documented form. HE blast tests were made against U.S. Army trucks, APCs, tank tracks and bottoms, fixed-wing and rotary-type aircraft, and various missile structural components. Figure 9 shows preparation for the test of blast effects from an 18.25-lb cylindrical Pentolite charge at a standoff of 10 ft from the skin of a B-57 aircraft. Figure 10 shows the sustained blast damage, and Figure 11 shows a closeup view of the test damage. Five HE blast-damage tests were made on B-57 aircraft. The test results and data

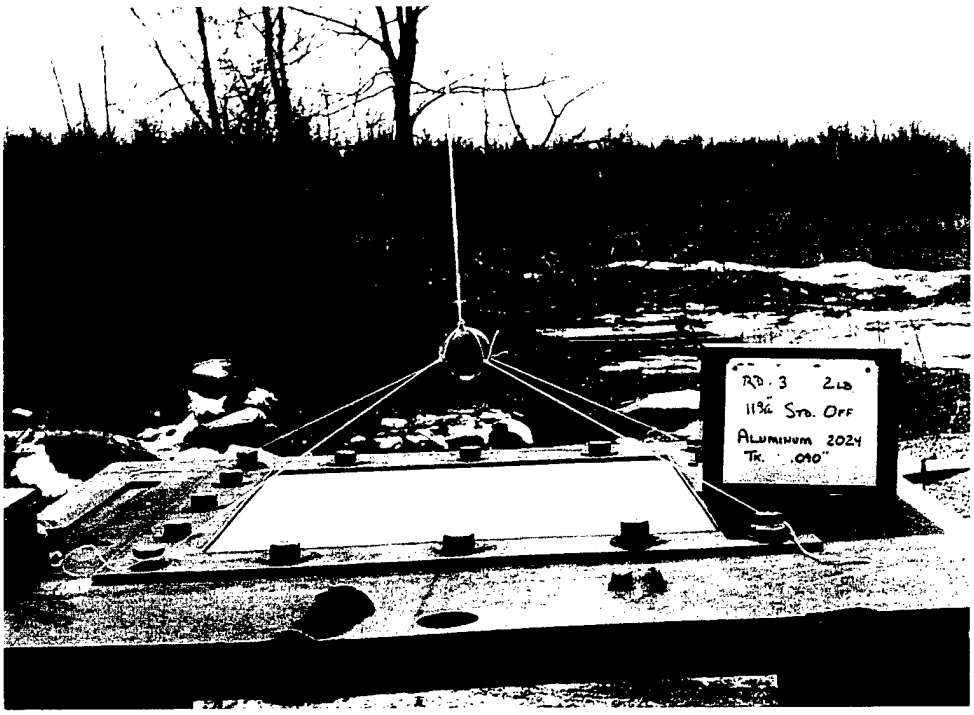

Figure 6a. Pretest Setup of a 0.090-in-Thick Aluminum 2024 Plate at an 11 9/16-in Standoff From a 2-lb Spherical Pentolite Charge.

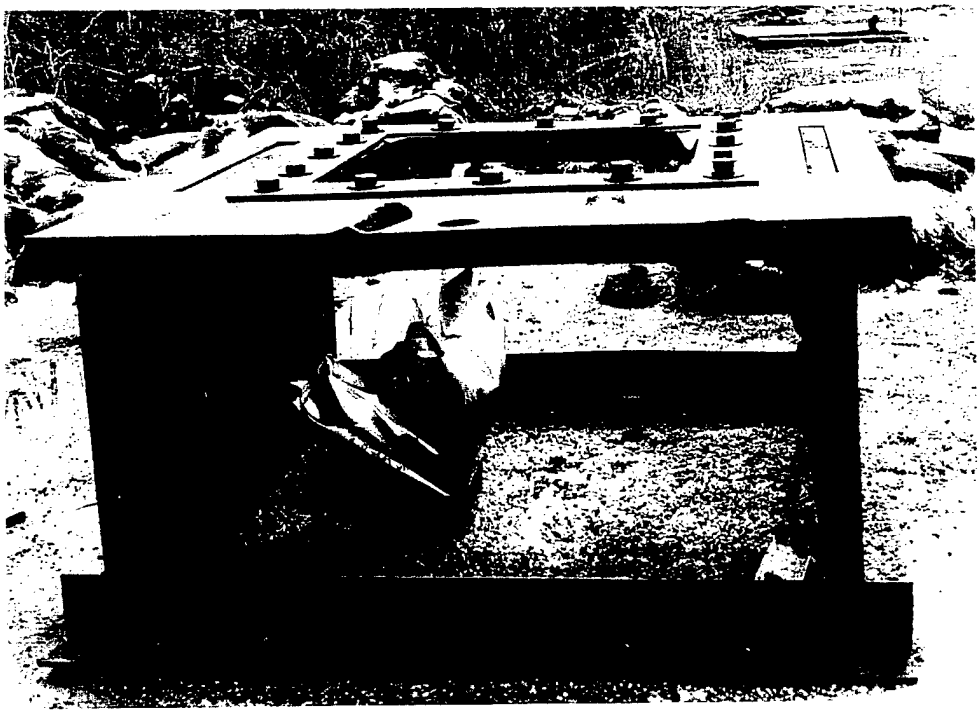

Figure 6b. After-Test Damage to a 0.090-in-Thick Aluminum 2024 Plate Due to the Blast From a 2-lb Spherical Pentolite Charge at an 11 9/16-in Standoff.

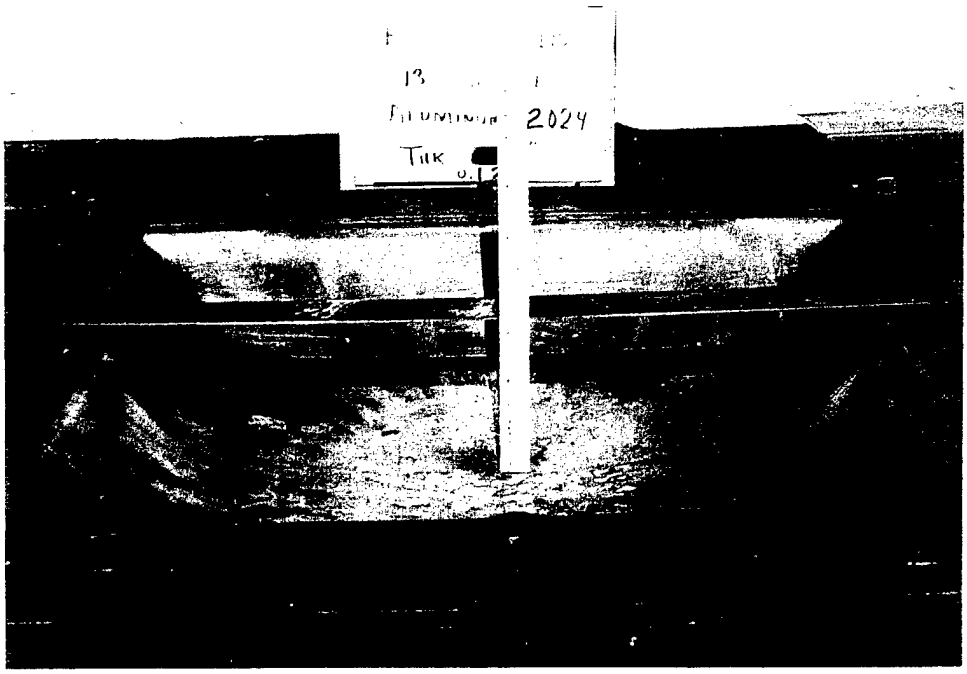

Figure 7. Damage to a 0.125-in-Thick Aluminum 2024 Plate Due to the Blast From a 2-lb Spherical Pentolite Charge at a 13-in Standoff.

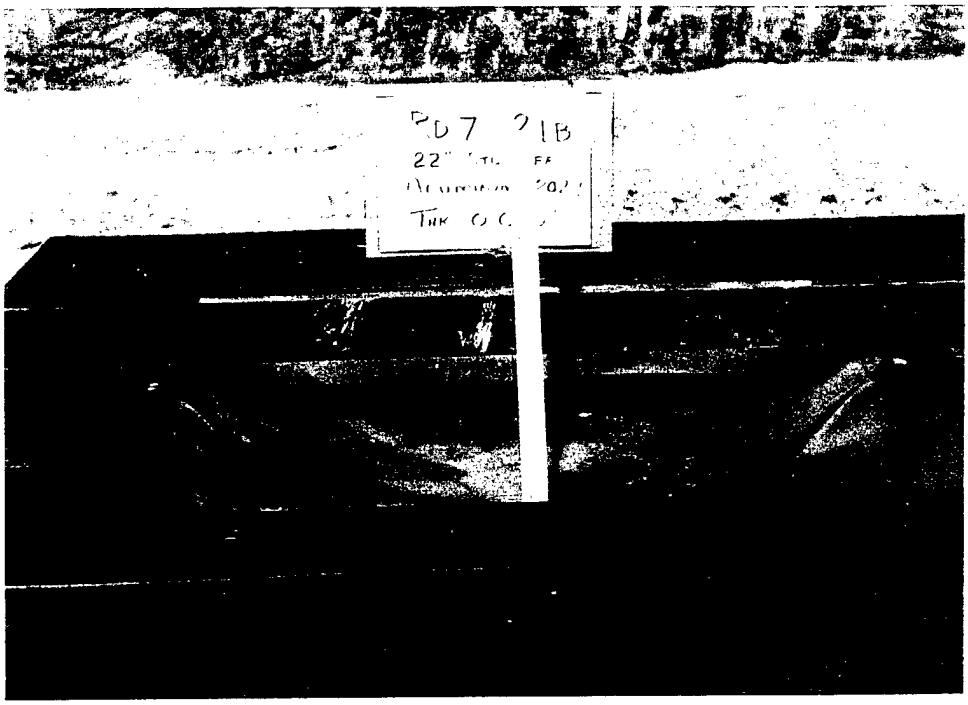

Figure 8. Damage to a 0.090-in-Thick Aluminum 2024 Plate Due to the Blast From a 2-lb Spherical Pentolite Charge at a 22-in Standoff.

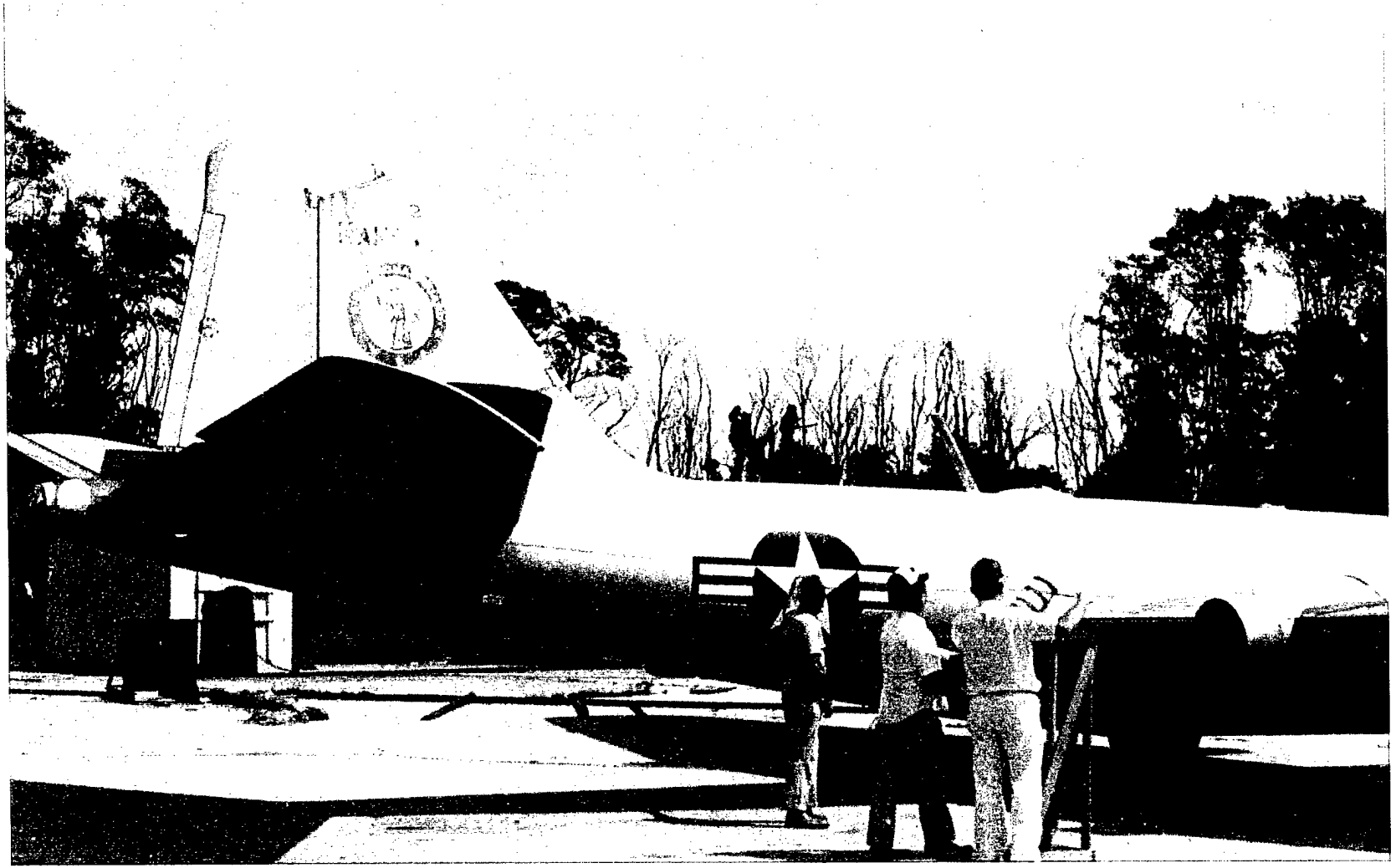

Figure 9. Preparations for Blast Test of an 18.25-lb Bare Pentolite Cylinder Charge vs. B-57 Aircraft at a 10-ft Standoff.

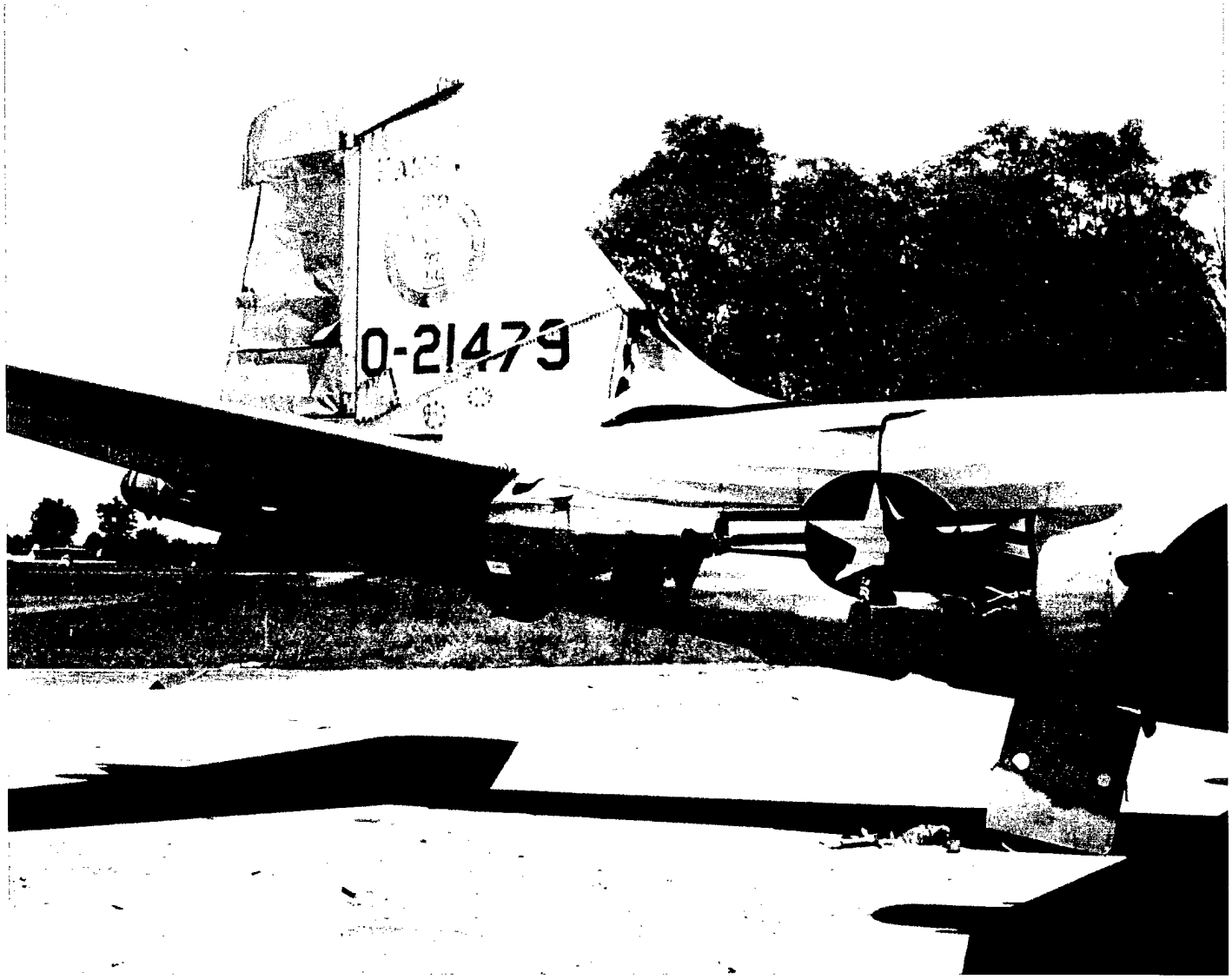

Figure 10. View of the Damage to the Right Side of a B-57 Aircraft Due to the Blast From an 18.25-lb Pentolite Cylinder Charge at a 10-ft Standoff.

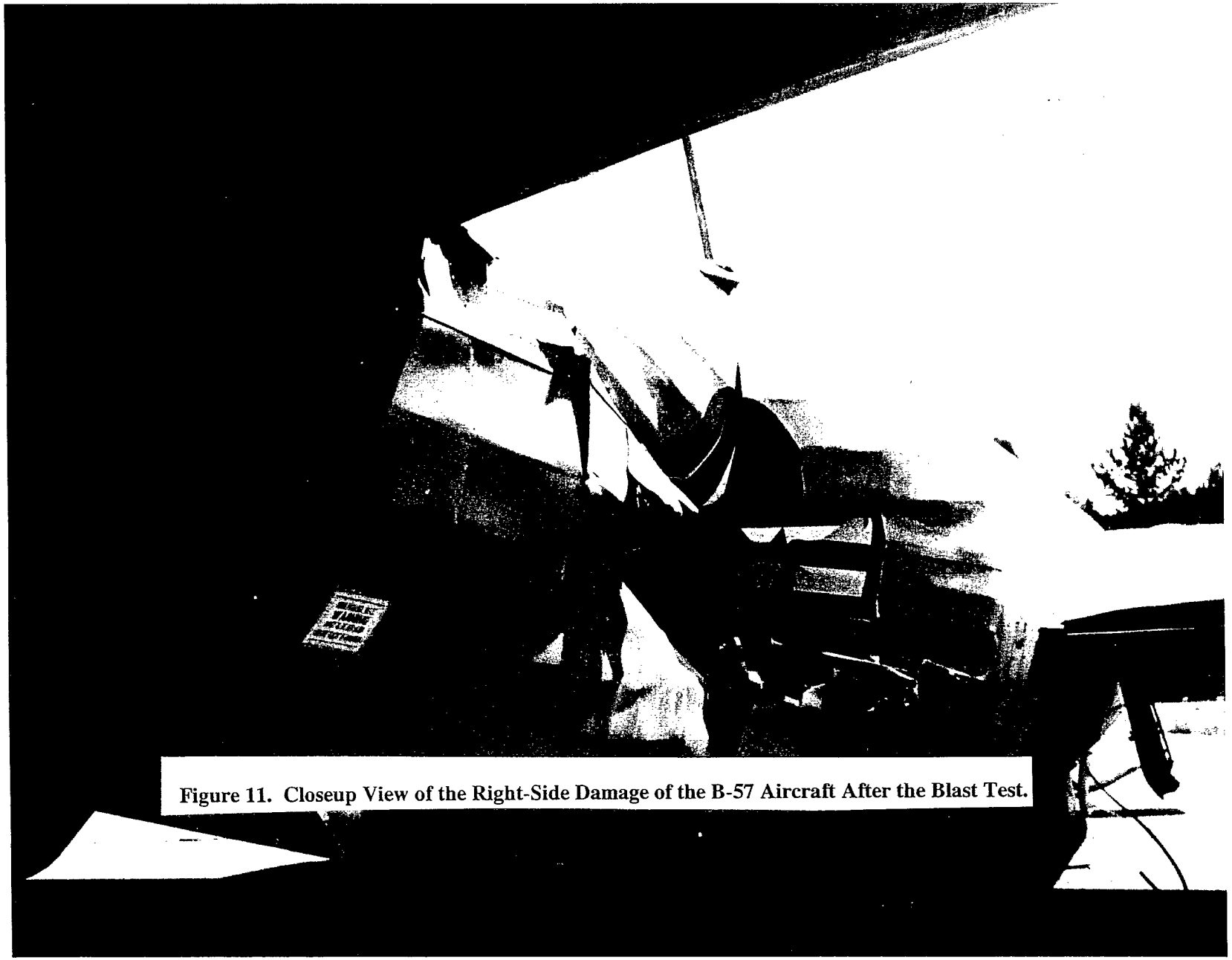

Figure 11. Closeup View of the Right-Side Damage of the B-57 Aircraft After the Blast Test.

analysis are shown in Mayerhofer, Kiwan, and Williams [18]. Figure 12 shows the damage sustained by an OH-58 helicopter due to the HE blast from an 8-lb spherical Pentolite charge detonated at a standoff of 7 ft 4 in from the skin of the cargo cabin door. Figure 13 shows the damage sustained by Hound Dog (AGM-28) missile engine inlet when subjected to the blast from a surface burst of an 8-lb spherical Pentolite charge at a distance of 7 ft from the skin of the inlet. The data from similar tests are in Kiwan [19]. Because HE blasts are more effective against light structures, extensive experimental blast data are available against various aircraft and missile structures. Test data of the Redeye missile (XM221) against various aircraft and missile structures can be found in the U.S. Army Test and Evaluation Command firing record R-3708 [20]. Damage data to the UH-1 helicopter from the blast of small C-3 charges are also available, as well as the blast damage data on a number of other aircraft. Finally, Figure 14 shows the damage sustained by scaled steel cylinders simulating chemical weapons containers due to the blast from a 20-lb cylindrical Pentolite charge.

4. HE Blast Damage Models

4.1 Blast Hole Model. Wolk and Wilner [21] developed a formula for the blast hole radius DR, in an armor plate of thickness T, due to the blast from an HE charge W, detonated at a standoff distance S from the plate. They assumed that an RHA plate of thickness T will fail when subjected to a critical overpressure P_c. Furthermore, they assumed that

$$P_c = a . T^b, \tag{12}$$

where a and b are constant parameters. By fitting the side-on overpressure data as a function of scaled distance, they derived an equation of the form

$$p = k . Z^d, \tag{13}$$

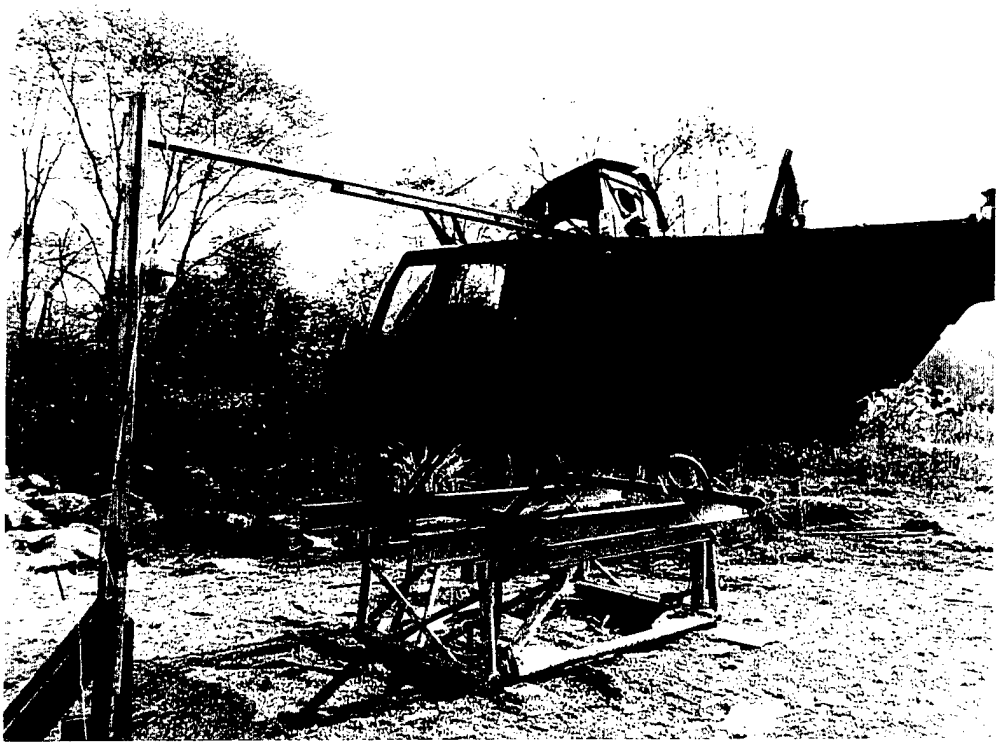

Figure 12a. Preparation for an HE Blast Test of an 8-lb Spherical Pentolite Charge vs. an OH-58 Helicopter at a 7-ft, 4-in Standoff.

Figure 12b. View of After-Blast Test Damage to the OH-58 Helicopter.

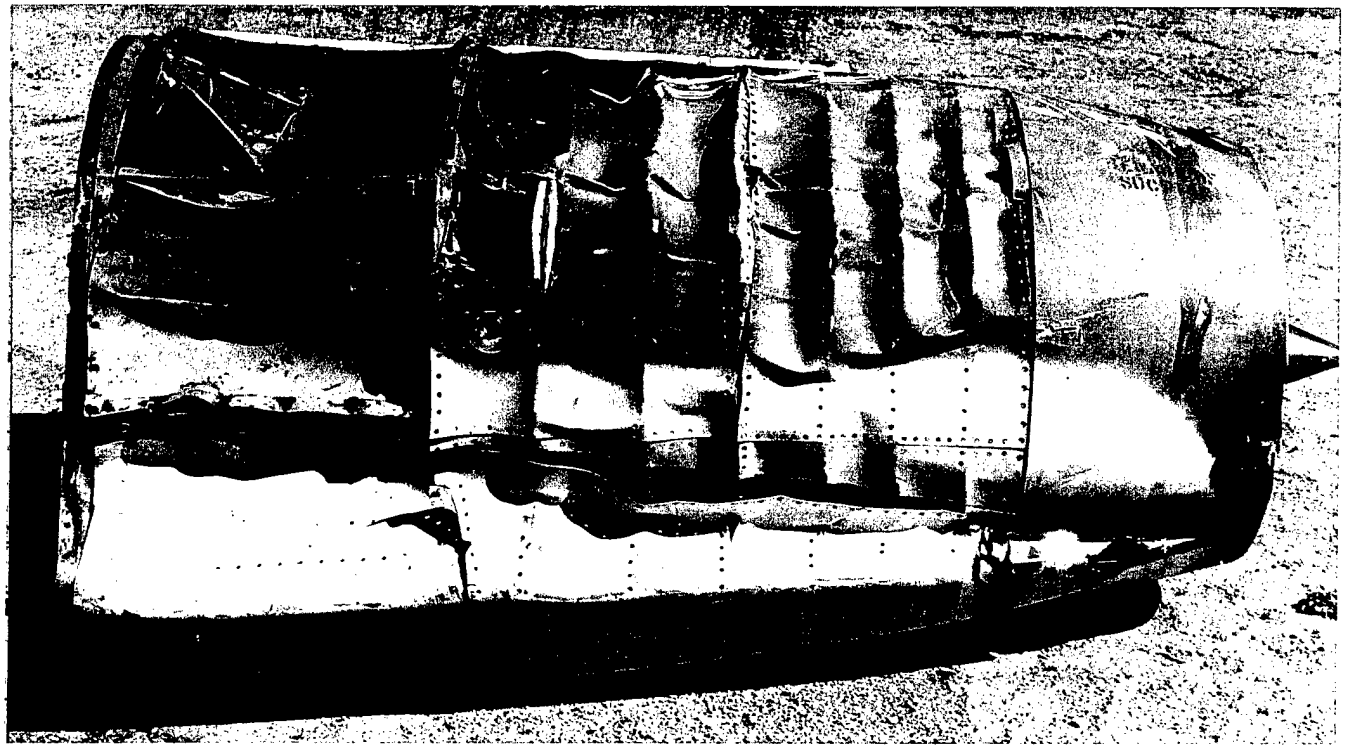

Figure 13. Damage to a Hound Dog Missile (AGM-28) Engine Inlet Due to the Blast From an 8-lb Surface Burst at a 7-ft Standoff.

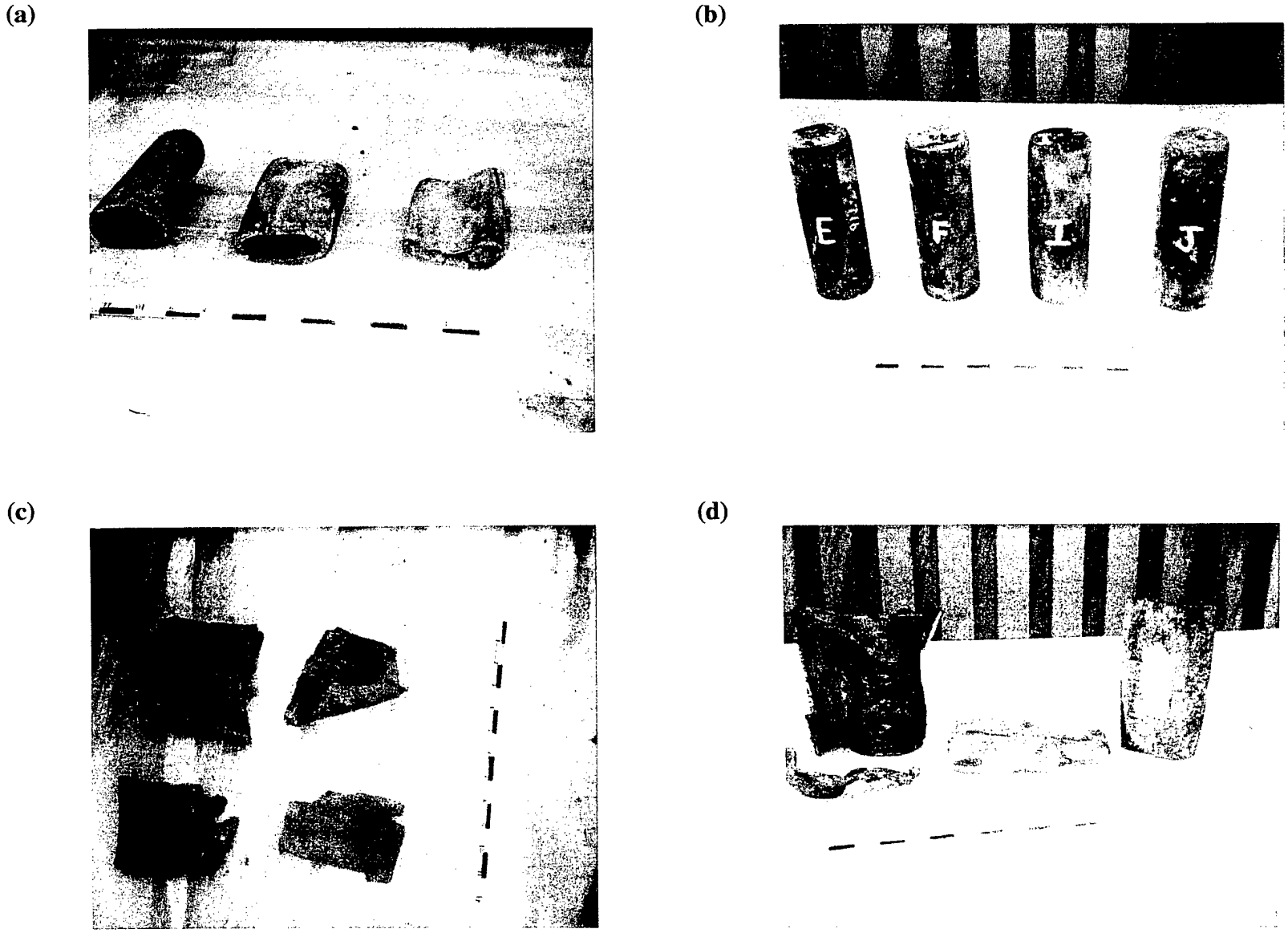

Figure 14. Damage to Scaled Steel Cylinders Due to the Blast From a 20-lb Pentolite Cylindrical Charge.

where k and d are constant parameters and

$$Z = R/W^{1/3}. \tag{14}$$

The blast from the charge W will generate a hole in the plate of radius DR, where the normal component of the blast overpressure is equal to the critical overpressure for that plate thickness T. By combining equations (12) and (13), they arrived at an equation for the blast hole radius DR as a function of W, S, and T. The formula can be expressed in functional form as:

$$DR = F(W, S, T). \tag{15}$$

Comparison of predictions from equation (15) with test results of holes generated by the blast from large bombs showed qualitative agreements. This model has been used in some ship vulnerability prediction codes.

4.2 RHA Plates Blast Damage Model. Kiwan used the experimental RHA test data for HE blast damage discussed in the previous section and documented in Kiwan and Goodman [14] in combination with similarity and dimensional analysis to derive a mathematical model for HE blast damage to RHA plates [22]. The analysis was later extended to apply to moving HE charges and documented in Kiwan [23]. The derived mathematical equations are

$$d = a \cdot W^{1.6458}/(T^{1.8796} \cdot S^{2.058}), \tag{16}$$

$$S_c = A^{0.2135} \cdot W^{0.5521}/T^{0.5149}, \tag{17}$$

and

$$DR = [A^2 \cdot W^{5.1716}/(S^{7.3669} \cdot T^{4.8233}) - S^2]^{0.5}, \tag{18}$$

where d denotes the maximum plate deformation, W, S, and T are the charge weight, the standoff of the charge center from the plate, and the plate thickness. a and A are constant parameters

whose values depend on the system of units used. S_c denotes the critical standoff for charge W, at which the plate fails and cracks appear.

$$a = 27392697 \quad \text{and} \quad A = 1.4478 \times 10^{11}, \tag{19}$$

when the millimeter is used for the unit of length and the kilogram is used for the unit of mass.

$$a = 0.8631 \text{ and } A = 2.0317, \tag{20}$$

when the inch and pound are used as units.

Predictions made with this model, as expressed with equations (16)–(18), compare well with the experimental data within the range of its validity, i.e.,

$$0.1875 <= T <= 0.75 \text{ in}, \tag{21}$$

and

$$2.0 <= W <= 8.0 \text{ lb}. \tag{22}$$

For more details on this model and comparison of predictions with experimental results, we refer the interested reader to Kiwan [22, 23].

4.3 Cylindrical Shells Blast Damage Model. Schuman conducted extensive experiments on the response of aluminum and steel cylindrical shells to blast loading. The data from these experiments were used to formulate a model for the damage to such shells [15, 16]. For lateral loading of cylinders by the blast wave, a critical overpressure P_c was determined for a shell to sustain a 5%–10% permanent deformation of its diameter. The required critical overpressure was found to be a function of the shell material, length-to-diameter ratio, shell diameter, thickness, and the charge weight. This functional dependence can be expressed by the equation:

$$P_{cr} = F_{L/D} \cdot F_D \cdot F_T \cdot F_w, \tag{23}$$

where $F_{L/D}$. F_D . F_T . and F_w are the factors for length-to-diameter ratio, the diameter, the shell thickness, and the charge weight. For a given case, these factors are determined from graphs that are given in Schuman [15]. For longitudinal loading of these shells, the required critical overpressure P_{cr} can be expressed as:

$$P_{cr} = g \cdot P_{cr}, \tag{24}$$

where g is a multiplication factor:

$$g = 6.0 \text{ for steel} \tag{25}$$

and

$$g = 2.0 \text{ for aluminum.} \tag{26}$$

This model has been used in missile vulnerability studies.

5. HE Blast Damage Scaling

5.1 The Johnson Relationship. Johnson [24] developed a relation between the explosive HE charge weight W, and the range R_w, at which a certain level of target response or damage due to the HE blast wave is achieved. Johnson examined the blast damage data for various types of targets (structures) and made the following observations. For each combination of charge weight W and distance R, one can associate values of pressure P and impulse I, and conversely. If one plots, for a given target or structure, the set of P and I data that will result in an equivalent level of damage, then such data fall on a curve similar to the one in Figure 15, which can be assumed to approximate a rectangular hyperbola. The target set that Johnson examined consisted of wire drag gauges, aluminum beams, aluminum cylinders, dish radar antenna, B-29 fuselage section, and 2-1/2-ton trucks. Johnson suspected that for a given target and level of response a relationship should exist between the explosive HE weight W, and the range R_w at which that level of response is achieved. Hence, by choosing an arbitrary but constant explosive weight and

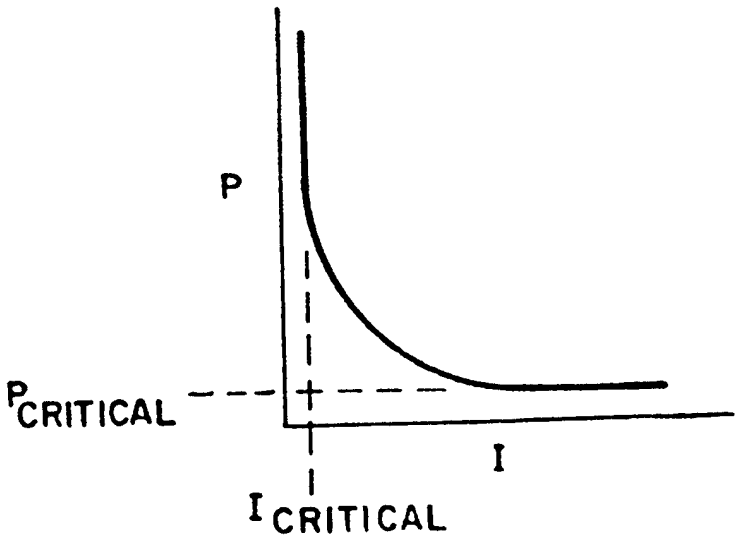

Figure 15. An Isodamage (Pressure-Impulse) Curve.

referencing all data to it, we should arrive at a constant range ratio for that weight W. For the constant weight, Johnson chose W = 100 lb and defined

$$C_w = R_{100}/R_w. \tag{27}$$

For the various considered targets, Johnson made a least-squares fit of C_w vs. W, to the functional form

$$C_w = a \cdot W^b. \tag{28}$$

Figure 16 shows the least-squares fit of the data used by Johnson. The a and b were determined to be 7.64 and −0.435. Equation (28) becomes:

$$C_w = 7.64\, W^{-0.435}. \tag{29}$$

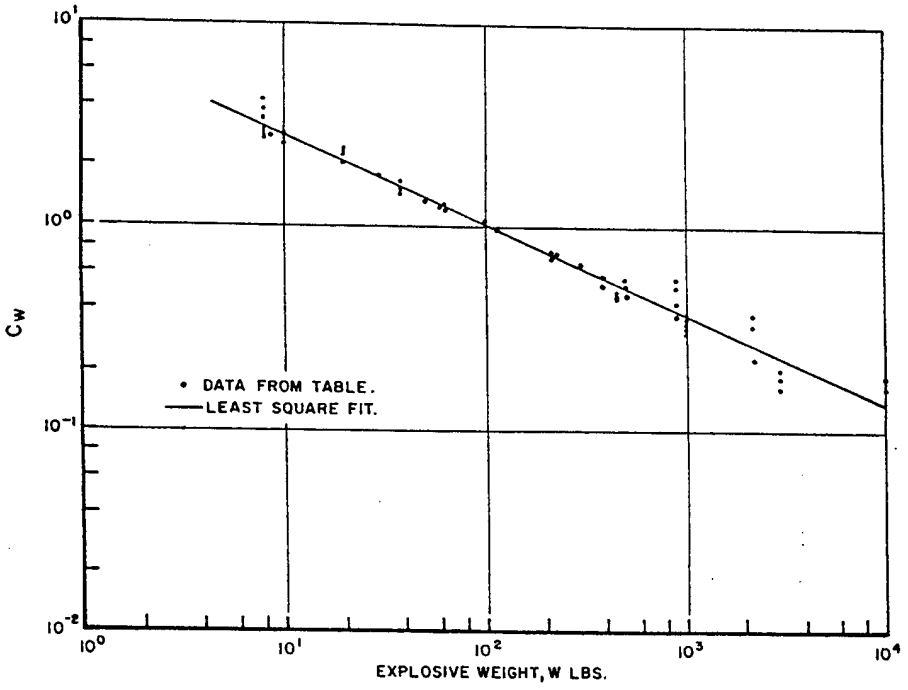

Figure 16. A Least-Squares Fit of C_w vs. Explosive Weight for an Arbitrary Response Level.

Let R_1, R_2 be the standoff distances corresponding to charge weights W_1 and W_2. Equation (29) then gives the scaling relationship:

$$R_1/R_2 = (W_1/W_2)^{0.435}. \tag{30}$$

Equation (30) can be used to scale from one vulnerability data point corresponding to charge weight W_1 to other charge weights. Equation (30) has been generalized to:

$$R_1/R_2 = (W_1/W_2)^c. \tag{31}$$

The value of the parameter c in equation (31) depends on the range of values of W_1 and W_2.

$c = 0.333$	for	W_i in the kiloton range
$c = 0.4$	for	$500\ lb < W_i <$ kiloton
$c = 0.435$	for	$10\ lb < W_i < 500\ lb$
$c = 0.49$	for	$1\ lb < W_i < 10\ lb$
$c = 0.6$	for	$W_i < 1\ lb$

(32)

5.2 Isodamage Curve Method. The concept of an isodamage curve expressed in terms of the parameters of peak overpressure P and impulse I was first proposed by Sperrazza [25]. This concept is based on the experimental observations that some parameters of the response of simple structures, such as cantilever beams, to transient loads such as maximum displacement, are a function of the peak load and impulse delivered to the target. Plots of the overpressure P vs. the impulse I data for equal values of maximum deflection fall on an isodamage curve similar to the one shown in Figure 15. Therefore, one can assume that such a relationship might hold for more severe damage of complex structures. It is possible to estimate for a given explosive weight W, a combination of overpressure P, and impulse I that will result in a specific level of damage to a target. The P - I curve shown in Figure 15 separates the plane into two distinct regions. Data points to the right of the curve represent loading that will cause more severe damage. Points to the left of the curve represent loading that will cause less severe damage to the structure. Greenspon [26] gave a theoretical analysis basis for the existence of isodamage P - I curves. The curve can be assumed to be hyperbolic and can be represented by the equation:

$$(P - P_{crit.})\,(I - I_{crit.}) = C. \tag{33}$$

C is a constant parameter whose value depends on the target's characteristics. $P_{crit.}$ and $I_{crit.}$ are two parameters representing the curve asymptotes. Determination of a specific isodamage curve requires three data points. However using the scaling relationship (equation 31) enables one to determine such a curve once we have a single data point. The P - I curve can be used to scale to other overpressure P and impulse I values that will result in the same level of damage to a given target.

5.3 Other Scaling Relationships. Equation (17) gives the critical standoff S_c for an HE charge of weight W from an RHA plate of thickness T in order for the plate to fail and crack due to the HE blast loading. One might suspect that this relation applies to other structures. Hence, dropping the subscript c and using numerical subscripts to describe parameters associated with various data sets, one deduces from equation (17) the following relations:

$$\text{For } T = \text{constant}, \quad S_1/S_2 = (W_1/W_2)^{0.5521}. \tag{34}$$

Equation (34) is a scaling relation analogous to equations (30) or (31). Equation (30) is based on a least-squares fit of the data set used by Johnson and documented in his BRL report [24], while equation (34) is based on the RHA plates data set documented in Kiwan and Goodman [14]. Equation (34) can be used to scale for a given target from one charge weight to another. Similarly, we can deduce from equation (17) the following relation:

$$\text{For } W = \text{constant}, \quad S_1/S_2 = (T_2/T_1)^{0.5149}. \tag{35}$$

Equation (35) can be used to scale from one target to another for the same constant charge weight W. Equations (34) and (35) have been used to scale experimental results of blast damage of steel cylinders to full-size submunition containers.

6. HE Blast Vulnerability Models

6.1 The Blast Correction Factor Method. R. Kirby and H. Ege attempted to account for the contribution made by HE blast loading, case fragments perforations, and transmitted shock from impacting explosive munitions to the vulnerability of lightly armored vehicles. Based on some combat data, they estimated the probability of kill due to these damage mechanisms as a function of the explosive charge weight of the munition and the mean armor thickness of the armored vehicle. This probability of kill denoted by P_{bcs} is shown in Figure 17. This probability

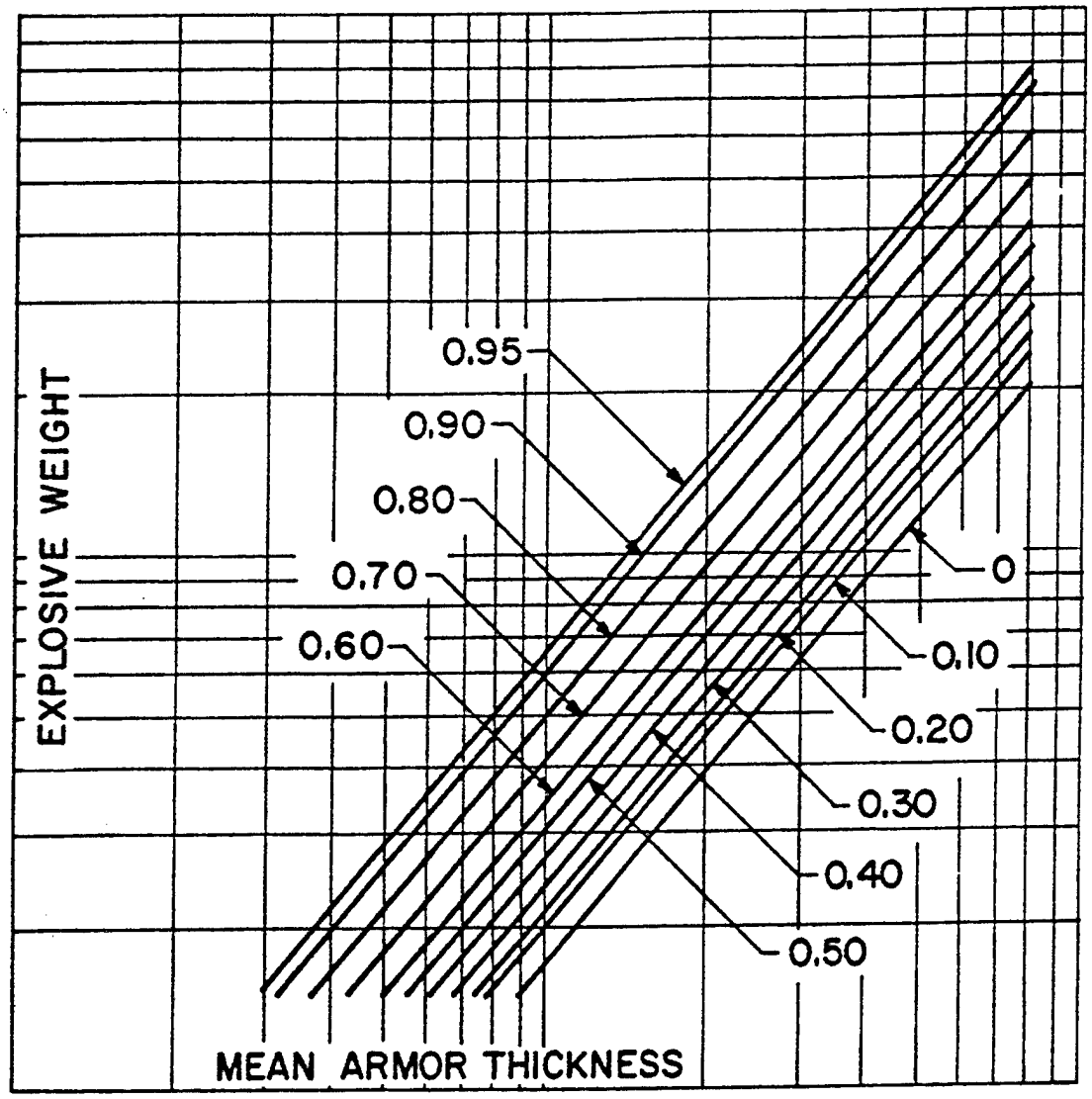

Figure 17. Probability of Kill, P_{bcs}, Due to Blast, Case Fragments, and Shock.

of kill is combined with the probabilities of kill for other damage mechanisms present, such as P_{sc}, the probability of kill due to the shaped charge jet through the survival rule. Thus one arrives at a total probability of kill P_{tot} for the munition.

$$P_{tot} = 1 - (1 - P_{sc})(1 - P_{bcs}) \tag{36}$$

This method of accounting for the contribution of blast effects to the vulnerability of armored vehicles provides quick vulnerability estimates to threat munitions. The main disadvantage of this method is the small amount of test data on which it is based.

6.2 The Critical Impulse in Critical Time Method. Robert Sewel of the U.S. Naval Ordnance Test Station (NOTS) formulated "A Blast Damage Criterion" and a vulnerability model for structures due to HE blast effects [27]. According to Sewel's model, a structure sustains permanent damage when a critical impulse is delivered to the structure in a critical time period. A formula is given for computing the critical impulse I_c:

$$I_c = V_c \cdot \rho \cdot T, \tag{37}$$

where I_c, V_c, ρ, and T are the critical impulse, critical impact velocity, and material density of the target and thickness, respectively. The critical impact velocity is related to the critical particle velocity in the material, which is that relative velocity between two particles in the material, and, if exceeded, causes the particles to behave as independent particles and no longer as part of the whole system. Furthermore, it was assumed that the critical time period during which the critical impulse needs to be delivered to the target to achieve the desired level of damage is pe/4, where pe is the period of the fundamental resonant frequency of the structure.

The application of this damage criterion in vulnerability studies was achieved by computing the side-on and the normally reflected impulse for the HE blast wave and assuming that:

$$\int_0^{pe/4} P_s \, dt > = I_c \quad \text{for } K_p = 1 \tag{38}$$

and

$$\int_0^{pe/4} P_r \, dt < = I_c \quad \text{for } K_p = 0, \tag{39}$$

where P_s = side-on pressure, psi, P_r = reflected pressure, and psi and pe/4 are the quarter period in milliseconds. Whenever $pe/4 > T^+$, the integration is taken to T^+, the time of positive duration of the blast wave, t = time. K_p = kill probability due to HE blast. Equations (38) and (39) define the 100% and 0% kill-level probabilities. Once the radii where the side-on and reflected impulse equal the critical impulse I_c are determined, these radii are defined as the 100% and 0% kill probabilities. A straight line is drawn between those two data points in the (R, K_p) plane, where R is the radial distance. Sewel used this model and computed the probabilities of kill for a number of military systems due to the blast from large HE bombs. Computations were made for a parked aircraft, a gun laying radar target, a missile control radar, a truck, an APC, and a tank. The bombs used in the calculation were the 250-lb MK-81, the 500-lb MK-82, and the 1000-lb MK-83, and the U.S. Air Force (USAF) 750-lb T-54 bomb. Experimental values of parameters were used in the calculations when available. Values for the remaining parameters were obtained from tables or theory. The critical impact velocity V_c was assumed to be 200 ft/s for steel and 300 ft/s for aluminum. Here we present some of the results of these calculations as reported by Sewell [27]. Figures 18–21 show the results of the computation for four of these targets.

Application of the Sewel model proved to be complicated. Computation of the critical impulse and time for a given target proved to be a difficult task. Similarly, the estimation of the critical particle velocity for a given material is not an easy task. These parameters often had to be determined from experiments that are rather costly and defeat the purpose of the method.

6.3 Blast Kill Radius Method. Researchers at the Naval Surface Warfare Center (NSWC) formulated an empirical method for calculating blast kill radii for missiles. The method is based on test data to determine the blast-critical impulse threshold for obtaining catastrophic structural kill of a missile and applying free-air blast-measured relationships for Pentolite charges to determine where the required critical impulse could be obtained. A brief description of the method, assumptions made, and the computational steps will be given as follows.

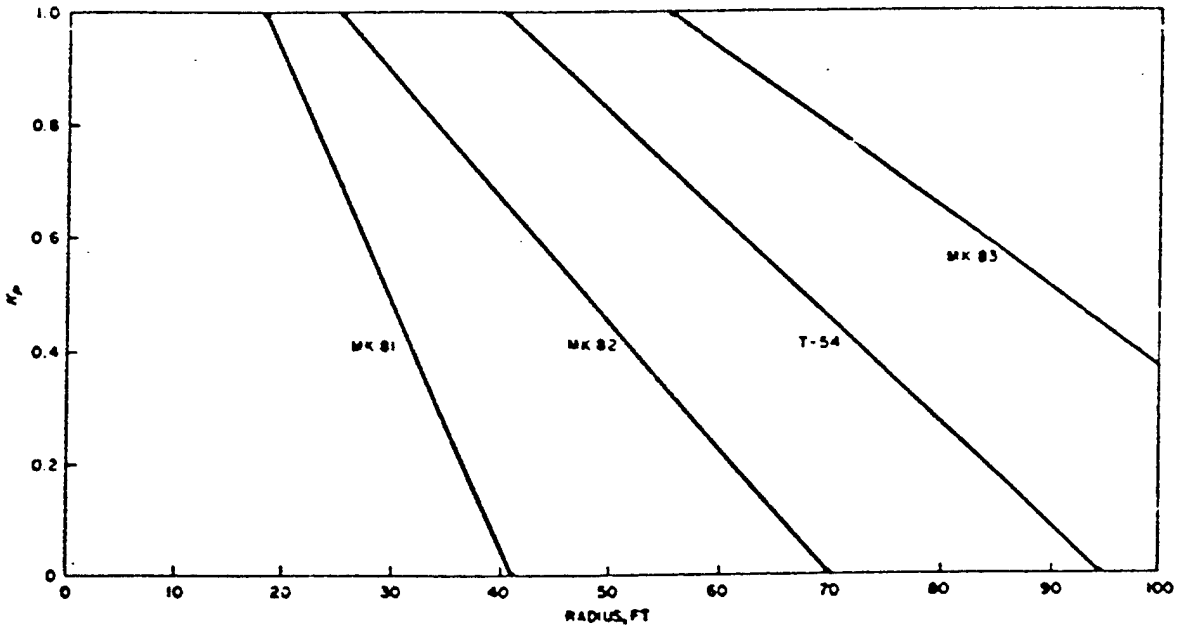

Figure 18. Kill Probability vs. Distance for Parked Aircraft Target.

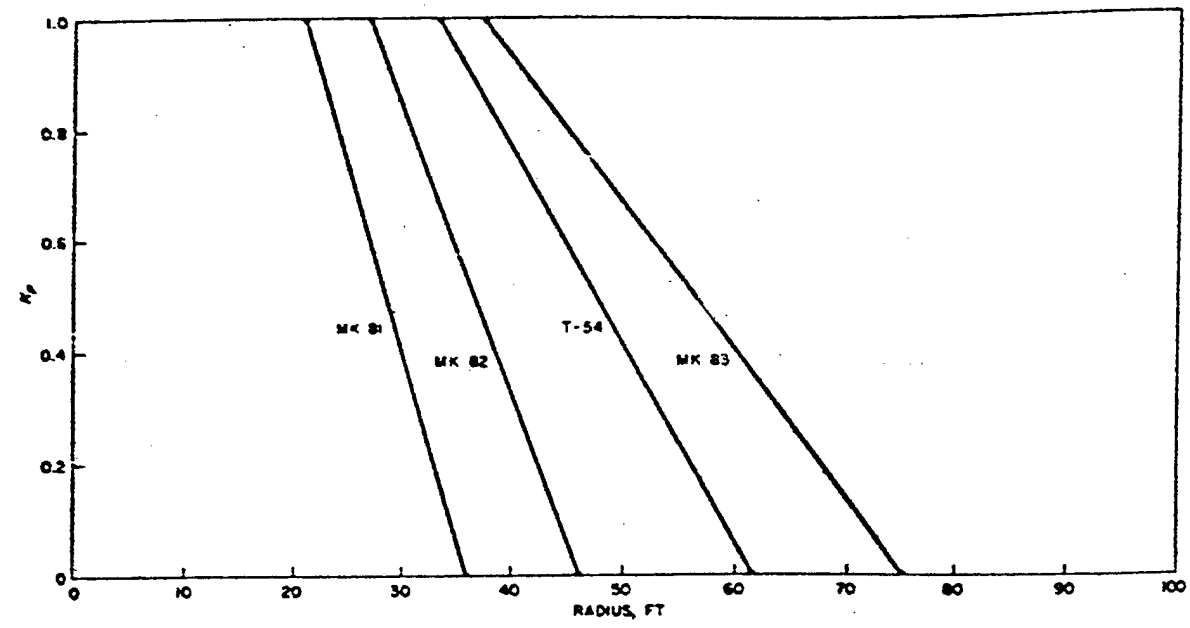

Figure 19. Kill Probability vs. Distance for Gun-Laying Radar Target.

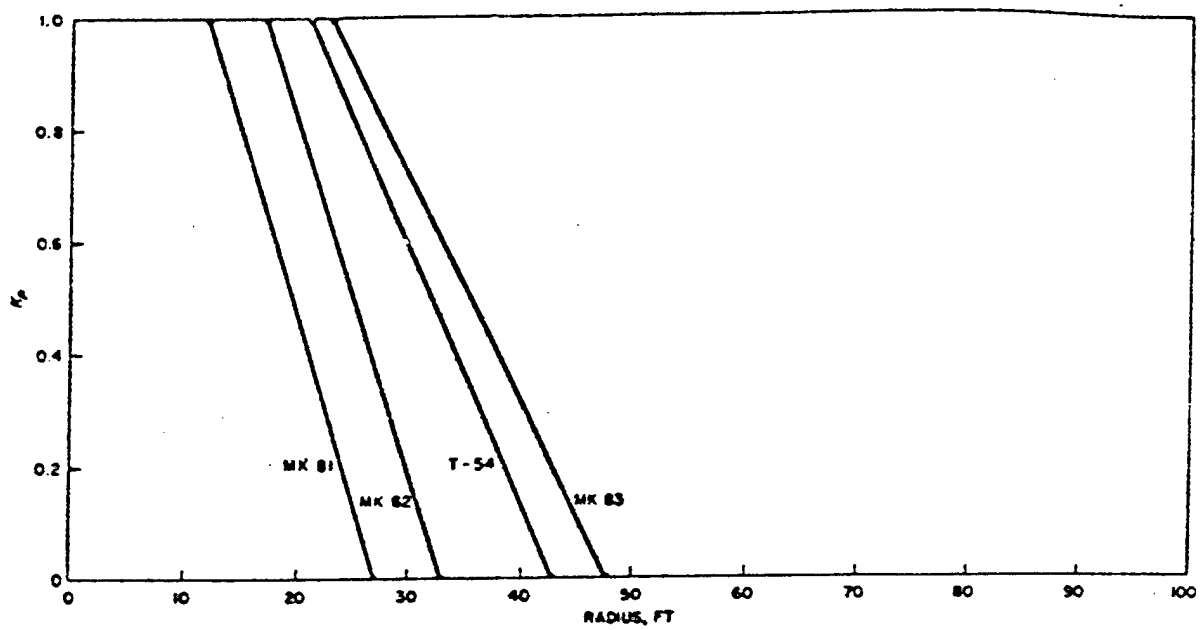

Figure 20. Kill Probability vs. Distance for Truck Target.

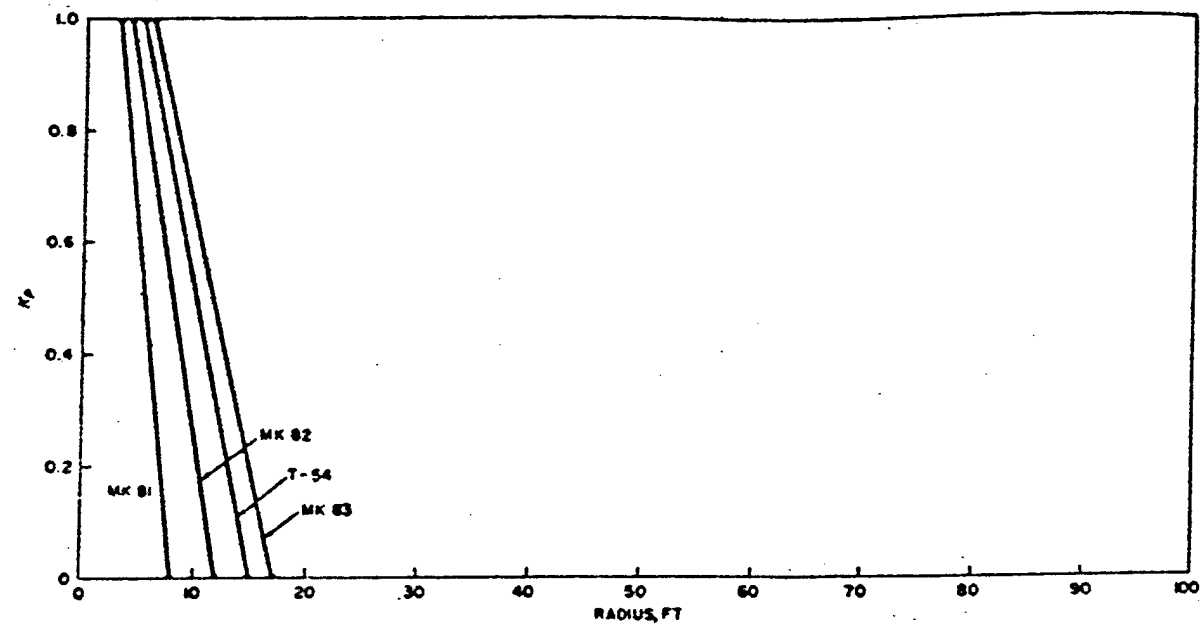

Figure 21. Kill Probability vs. Distance for Tank Target.

Based on the review of test data [28, 29, 30], it was assumed that the critical damage required to provide a structural kill of a missile and cause loss of control and ground impact within 30 s is rupture of the missile's skin. Based on test data for air targets with skin thicknesses in the range of 0.040–0.075 in, it was determined that a reflected impulse of 100–180 psi-m/s is required to cause skin rupture in this range of thicknesses. A fit of the experimental test data of critical impulse vs. skin thickness for targets with aluminum skin gave the following relationship:

$$I_c = 2709 \, . \, T \text{ psi-m/s.} \tag{40}$$

Equation (40) is approximately correct. T is the skin thickness in inches. In order to use this equation in vulnerability assessments to a threat, one has to determine first the equivalent bare charge weight, W_e, of the threat. W_e can be determined from the modified Fanno formula:

$$W_e = \text{Explosive Weight } [0.6 + 0.4 \, (1 + 2 \text{ Case Weight/Explosive Weight})^{-1}]. \tag{41}$$

Next, one calculates the scaled critical impulse of the target and equates it to the scaled reflected impulse.

$$2709 \, . \, T/W_e^{1/3} = I/W^{1/3} \tag{42}$$

From the curves for scaled impulse data for the geometry of the threat charge, one determines the scaled distance at which this impulse is achieved. The lethal blast kill radius is then defined as:

$$R = (R/W^{1/3}) \, (W_e^{1/3}). \tag{43}$$

This method can be used to provide quick approximate estimates of blast kill radii for aircraft and missiles in the absence of test data.

6.4 The Lethal Blast Contours Method. Historically, the vulnerability of an aircraft to the blast from an HE projectile was represented by defining a three-dimensional volume around the

aircraft, such that a kill of the aircraft occurs if the HE charge detonates inside that volume. Visualization of this volume (termed the lethal blast volume) was achieved by taking plane cross sections through the aircraft and the surrounding volume. The contour created by the intersection of the plane and the lethal volume is termed the lethal blast contour. Mayerhofer (formerly of BRL) formalized this process for aircraft by constructing such contours in four orthogonal planes. Three of the planes are mutually orthogonal. These planes are usually designated as A, B, C, and D. Plane D contains the aircraft main axis and is parallel to the wing span. Plane C also contains the aircraft main axis and is perpendicular to plane D. Plane A is perpendicular to the aircraft main axis, but intersects some critical components or subsystems in the forward section of the aircraft such as the crew compartment or the wing span. Plane B is parallel to plane A but intersects some critical components or subsystems in the rear of the aircraft such as the horizontal or vertical stabilizer.

The computation of the lethal blast contours in these coordinate planes A, B, C, and D for an HE charge W is accomplished as follows: For the kill category under consideration, an analysis is conducted that identifies the aircraft critical components for that category that can be killed by the external blast. For HE-blast kills, the aircraft structure is considered a critical component. Next, for each of the critical components, a determination is made of the type and extent of damage that will produce a complete dysfunction of that component. For the plane under consideration and each of the critical components that can be damaged by the detonation of the HE charge W, in the plane or a small neighborhood of it, one determines the maximum radial distance from the component at which such a detonation results in the desired level of damage. This radial distance is defined as the lethal blast radius R for that component. At each of these critical components, a circular arc of radius R is drawn. The lethal blast contour in the plane is obtained by drawing the envelop of these arcs. The lethal blast volume is the envelop generated by all such contours. Figures 22–24 show the lethal blast contours for the AH-1Q helicopter and for a series of TNT charges drawn in planes A, B, C, and D.

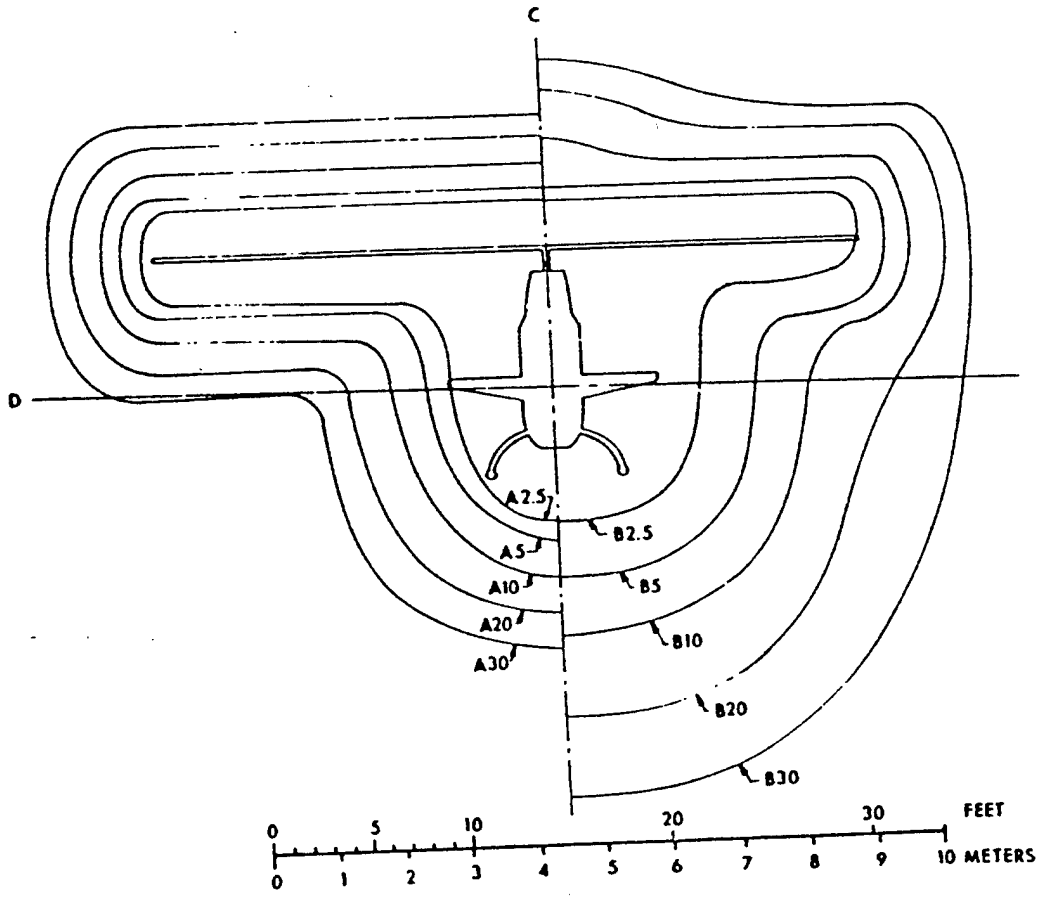

Figure 22. AH-1Q Attrition Kill External Blast Contours at Sea Level for Equivalent Charge Weights 2.5-, 5-, 10-, 20-, and 30-lb TNT; A/B Plane.

7. Conclusions

The previously described methods give a brief overview of HE blast phenomenology, HE blast damage mechanisms, the vulnerability of structures to HE blast, and vulnerability assessment methods. The subjects of material failure and damage assessments are highly complex and are poorly understood. A considerable amount of research of material failures to various damage mechanisms is being conducted especially on composite materials. Unfortunately, very little support is being provided for studying material failure and damage due to HE blast damage mechanisms. This report gives a brief description of empirical and engineering methods of HE blast damage and assessment methods but does not describe any computer codes that exist on the subject. However, this report states that the accuracy of

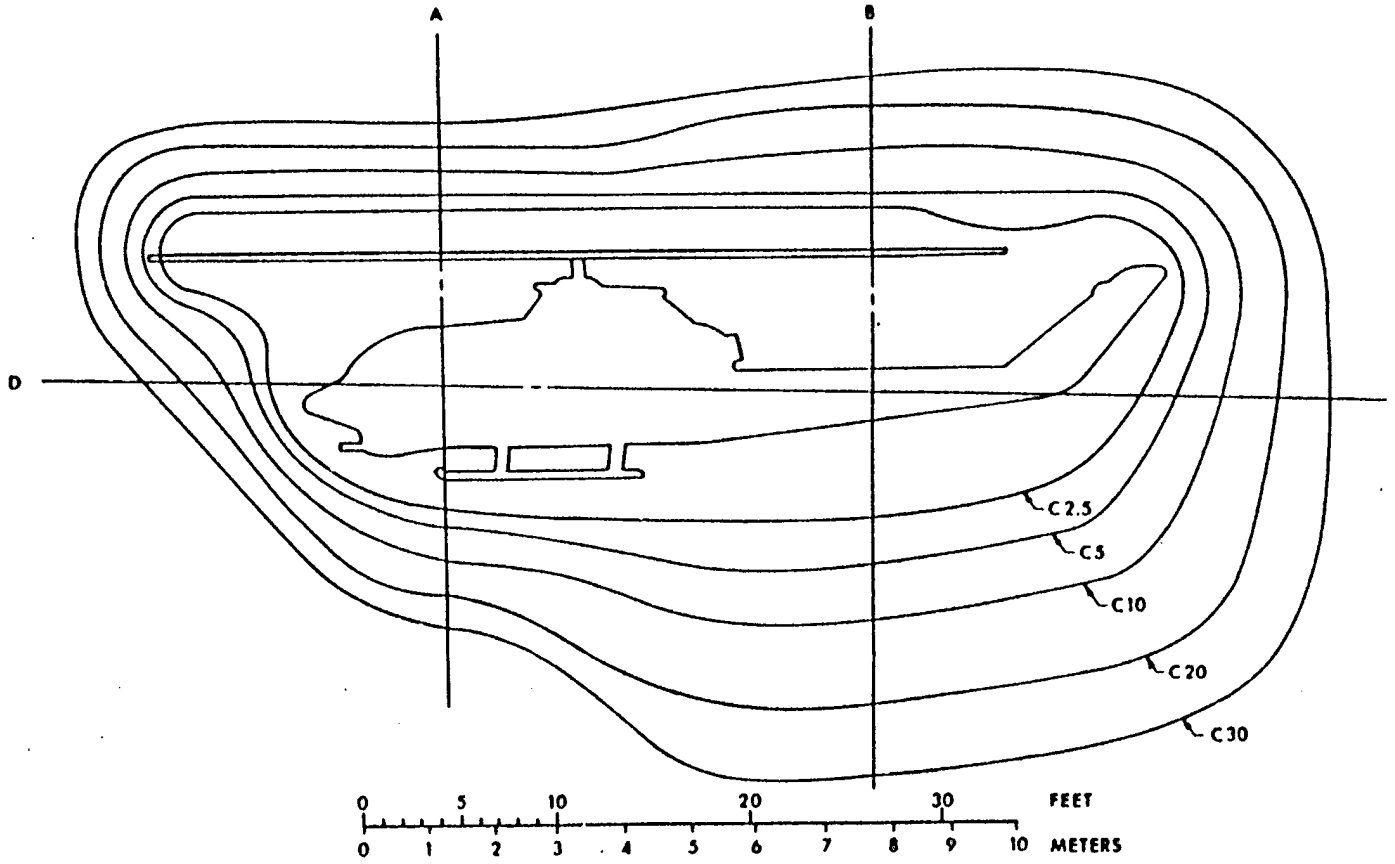

Figure 23. AH-1Q Attrition Kill External Blast Contours at Sea Level for Equivalent Charge Weights 2.5-, 5-, 10-, 20-, and 30-lb TNT; C Plane.

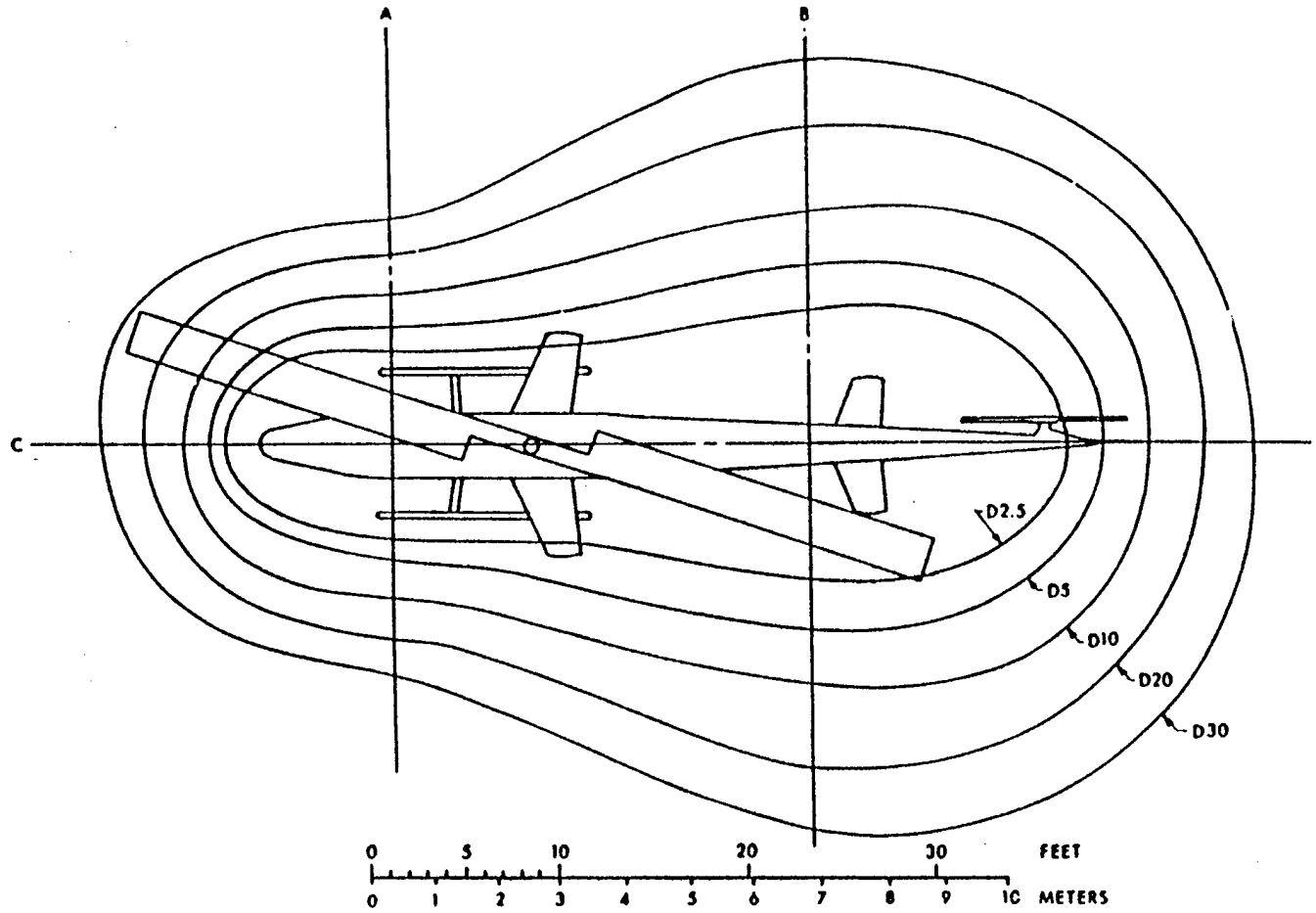

Figure 24. AH-1Q Attrition Kill External Blast Contours at Sea Level for Equivalent Charge Weights 2.5-, 5-, 10-, 20-, and 30-lb TNT; D Plane.

continuum mechanics codes in simulating such problems relies upon the material failure criterion contained in the code and how closely it simulates material behavior under these loading conditions. The aforementioned account is by no means inclusive of all available models and methods. The author mentions here, in passing, a model for material failure of tank bottoms due to a mine blast formulated by Haskell [31] that is based on energy considerations.

8. References

1. Swisdak, M. M., Jr. "Explosion Effects and Properties, Part 1 - Explosion Effects in Air." NSWC/WOL/TR 75-1162, Naval Surface Warfare Center, White Oak, Silver Spring, MD, October 1975.

2. Goodman, H. J. "Compiled Free-Air Blast Data on Bare Spherical Pentolite." Report No. 1092, U.S. Army Ballistic Research Laboratory, Aberdeen Proving Ground, MD, 1960.

3. Shear, R. E., and A. L. Arbuckle. "Calculated Explosive and Blast Properties for Selected Explosives." 61JTCG/ME-70-10, vol. 3, annex 7, Joint Technical Coordinating Group for Munitions Effectiveness, Explosive Steering Committee, Aberdeen Proving Ground, MD, June 1971.

4. U.S. Army Materiel Command. *Engineering Design Handbook - Explosive Series, Properties of Explosives of Military Interest.* AMC Pamphlet 706-177, Alexandria, VA, January 1971.

5. Ethridge, N. H. "A Procedure for Reading and Smoothing H. E. and Nuclear Explosives." BRL Memo Report 1691, Aberdeen Proving Ground, MD, September 1965.

6. U.S. Army Materiel Command. *Engineering Design Handbook - Explosive Series, Explosions in Air, Part 1.* AMC Pamphlet 706-181, Alexandria, VA, 15 July 1974.

7. Baker, W. E. *Explosions in Air.* Austin, TX: University of Texas Press, 1973.

8. Doering, W., and G. Burkhardt. "Contributions to the Theory of Detonation." TR No. F-TS-1227-1A, Wright-Patterson Air Force Base, OH, May 1949.

9. Shear, R., and P. McCane. "Normally Reflected Shock Front Parameters." BRL-MR-1273, U.S. Army Ballistic Research Laboratory, Aberdeen Proving Ground, MD, May 1960.

10. Courant, R., and K. O. Friedrichs. *Supersonic Flow and Shock Waves.* New York: Interscience Publishers, 1948.

11. Sachs, R. G. "The Dependence of Blast on Ambient Pressure and Temperature." Report No. 466, U.S. Army Ballistic Research Laboratory, Aberdeen Proving Ground, MD, 1944.

12. Sperrazza, J. "Modeling of Air Blast - Use of Models and Scaling in Shock and Vibration." American Society of Mechanical Engineers, New York, NY, edited by W. E. Baker, November 1963.

13. Dewey, J. M., and J. Sperrazza. "The Effect of Atmospheric Pressure and Temperature on Air Shock." BRL-TR-721, U.S. Army Ballistic Research Laboratory, Aberdeen Proving Ground, MD, 1950.

14. Kiwan, A. R., and H. J. Goodman. "The Response of Rolled Homogeneous Steel Armor Plates to Explosive Blast Loading." BRL-TR-02393, U.S. Army Ballistic Research Laboratory, Aberdeen Proving Ground, MD, February 1982.

15. Schuman, W. J., Jr. "The Response of Cylindrical Shells to External Blast Loading, Part II." BRL-MR-1560, U.S. Army Ballistic Research Laboratory, Aberdeen Proving Ground, MD, May 1964.

16. Schuman, W. J., Jr. "A Failure Criterion for Blast Loaded Cylindrical Shells." BRL-R-1292, U.S. Army Ballistic Research Laboratory, Aberdeen Proving Ground, MD, May 1965.

17. Baker, W. E., et al. "The Elastic and Plastic Response of Cantilevers to Air Blast Loading." Report No. 1121, U.S. Army Ballistic Research Laboratory, Aberdeen Proving Ground, MD, December 1960.

18. Mayerhoffer, R. D., A. R. Kiwan, and J. S. Williams. "Conceptual and Experimental Investigation of Aircraft Vulnerability Methodology for Attacks by Combined Blast and Fragment Warheads." BRL-IMR-852, U.S. Army Ballistic Research Laboratory, Aberdeen Proving Ground, MD, September 1966.

19. Kiwan, A. R. "Blast/Fragment Warhead Parameters Tradeoff for Increased Warhead Lethality." ARL-TR-175, U.S. Army Ballistic Research Laboratory, Aberdeen Proving Ground, MD, August 1993.

20. U.S. Army Test and Evaluation Command. *Firing Record R-3708.* TECOM Project No. 3-4-0201-22, Aberdeen Proving Ground, MD, 22 September 1966.

21. Wolk, H. L., and A. R. Wilner. "Predicting Blast Hole Size." NSRDC Report C-388, Naval Ship Research and Development Center, Bethesda, MD, 1972.

22. Kiwan, A. R. "Experimental and Analytical Study of the Response of Clamped Rolled Homogeneous Steel Armor to Close-In Blast Loading." BRL-TR-02509, U.S. Army Ballistic Research Laboratory, Aberdeen Proving Ground, MD, July 1983.

23. Kiwan, A. R. "The Vulnerability of Light Steel Armor to Close-In Blast Loading From Static or Moving Charges." BRL-TR-02587, U.S. Army Ballistic Research Laboratory, Aberdeen Proving Ground, MD, August 1984.

24. Johnson, O. T. "A Blast-Damage Relationship." Report No. 1389, U.S. Army Ballistic Research Laboratory, Aberdeen Proving Ground, MD, September 1967.

25. Sperrazza, J. "Dependence on External Blast Damage to A-25 Aircraft on Peak Pressure and Impulse." BRL-MR-575, U.S. Army Ballistic Research Laboratory, Aberdeen Proving Ground, MD, April 1952.

26. Greenspon, J. W. "Prediction of ISO-Damage Curves." J. G. Engineering Technical Report No. 8, Baltimore, MD, July 1967.

27. Sewel, R. G. S. "A Blast Damage Criterion." NOTS-TP-3426, Naval Ordnance Test Station, China Lake, CA, March 1964.

28. Naval Surface Weapons Center. "External Blast Vulnerability Tests of Aircraft Flaps and Vertical Stabilizers." NSWC-TR-79-236, Dahlgren, VA, August 1979.

29. Ford, R. T. "Blast Vulnerability of the AF-9J Aircraft." NSWC/DL-TR-3631, Naval Surface Weapons Center, Dahlgren, VA, November 1978.

30. Falcon Research and Development Company. "Blast Effects." Denver, CO, December 1974.

31. Haskell, D. F. "Deformation and Fracture of Tank Bottom Hull Plates Subjected to Mine Blast." Report No. 1587, U.S. Army Ballistic Research Laboratory, Aberdeen Proving Ground, MD, May 1972.

INTENTIONALLY LEFT BLANK.

List of Symbols

τ, ζ	Scaled time and scaled impulse.
d	Maximum plate deformation.
DR	Blast hole radius.
E	Total energy.
$F_{L/D}, F_D, F_t, F_W$	Factors of length-to-diameter ratio, diameter, thickness, and weight.
I_c, V_c	Critical impulse and critical impact velocity.
$I^{(h)}, a_0^{(h)}$	Overpressure and ambient atmosphere sound speed at altitude h.
$I_s^+, (I_s^-)$	Positive (negative) side-on impulse.
K_p	Kill probability.
$p_0, \rho_0, \theta_0, a_0$	Ambient atmospheric pressure, density, temperature, and sound speed.
P_{bcs}	Probability of kill due to blast, case fragments, and shock.
P_c, P_{cr}	Critical overpressure.
pe	Period of the natural resonant frequency for the structure.
$P_r, \rho_r, \theta_r, u_r$	Overpressure, density, temperature, and particle velocity behind the reflected wave front.
$P_s^+, (P_s^-)$	Peak side-on positive (negative) phase overpressure.
$P_s, \rho_s, \theta_s, u_s$	Free air side-on pressure, density, temperature, and particle velocity.
P_{sc}	Probability of kill due to shaped charge jet.
p(t)	Overpressure at time t.
P_{tot}	Total probability of kill.
R	Radial distance.

S, S_c	Standoff distance and critical standoff distance.
T	Plate or skin target thickness.
t, t_a	Time variable and time of arrival of the wave.
$T^+, (T^-)$	Time of positive (negative) duration of the wave.
W	Explosive weight.
Z	Scaled distance.

NO. OF COPIES	ORGANIZATION
2	DEFENSE TECHNICAL INFORMATION CENTER DTIC DDA 8725 JOHN J KINGMAN RD STE 0944 FT BELVOIR VA 22060-6218
1	HQDA DAMO FDQ DENNIS SCHMIDT 400 ARMY PENTAGON WASHINGTON DC 20310-0460
1	CECOM SP & TRRSTRL COMMCTN DIV AMSEL RD ST MC M H SOICHER FT MONMOUTH NJ 07703-5203
1	PRIN DPTY FOR TCHNLGY HQ US ARMY MATCOM AMCDCG T M FISETTE 5001 EISENHOWER AVE ALEXANDRIA VA 22333-0001
1	PRIN DPTY FOR ACQUSTN HQS US ARMY MATCOM AMCDCG A D ADAMS 5001 EISENHOWER AVE ALEXANDRIA VA 22333-0001
1	DPTY CG FOR RDE HQS US ARMY MATCOM AMCRD BG BEAUCHAMP 5001 EISENHOWER AVE ALEXANDRIA VA 22333-0001
1	DPTY ASSIST SCY FOR R&T SARD TT T KILLION THE PENTAGON WASHINGTON DC 20310-0103
1	OSD OUSD(A&T)/ODDDR&E(R) J LUPO THE PENTAGON WASHINGTON DC 20301-7100

NO. OF COPIES	ORGANIZATION
1	INST FOR ADVNCD TCHNLGY THE UNIV OF TEXAS AT AUSTIN PO BOX 202797 AUSTIN TX 78720-2797
1	DUSD SPACE 1E765 J G MCNEFF 3900 DEFENSE PENTAGON WASHINGTON DC 20301-3900
1	USAASA MOAS AI W PARRON 9325 GUNSTON RD STE N319 FT BELVOIR VA 22060-5582
1	CECOM PM GPS COL S YOUNG FT MONMOUTH NJ 07703
1	GPS JOINT PROG OFC DIR COL J CLAY 2435 VELA WAY STE 1613 LOS ANGELES AFB CA 90245-5500
1	ELECTRONIC SYS DIV DIR CECOM RDEC J NIEMELA FT MONMOUTH NJ 07703
3	DARPA L STOTTS J PENNELLA B KASPAR 3701 N FAIRFAX DR ARLINGTON VA 22203-1714
1	SPCL ASST TO WING CMNDR 50SW/CCX CAPT P H BERNSTEIN 300 O'MALLEY AVE STE 20 FALCON AFB CO 80912-3020
1	USAF SMC/CED DMA/JPO M ISON 2435 VELA WAY STE 1613 LOS ANGELES AFB CA 90245-5500

NO. OF
COPIES ORGANIZATION

1 US MILITARY ACADEMY
MATH SCI CTR OF EXCELLENCE
DEPT OF MATHEMATICAL SCI
MDN A MAJ DON ENGEN
THAYER HALL
WEST POINT NY 10996-1786

1 DIRECTOR
US ARMY RESEARCH LAB
AMSRL CS AL TP
2800 POWDER MILL RD
ADELPHI MD 20783-1145

1 DIRECTOR
US ARMY RESEARCH LAB
AMSRL CS AL TA
2800 POWDER MILL RD
ADELPHI MD 20783-1145

3 DIRECTOR
US ARMY RESEARCH LAB
AMSRL CI LL
2800 POWDER MILL RD
ADELPHI MD 20783-1145

ABERDEEN PROVING GROUND

3 DIR USARL
AMSRL CI LP (305)

NO. OF COPIES	ORGANIZATION
1	OSD OUSD AT STRT TAC SYS DR SCHNEITER 3090 DEFNS PENTAGON RM 3E130 WASHINGTON DC 20301-3090
1	ASST SECY ARMY RESEARCH DEVELOPMENT ACQUISITION SARD ZD RM 2E673 103 ARMY PENTAGON WASHINGTON DC 20310-0103
1	ASST SECY ARMY RESEARCH DEVELOPMENT ACQUISITION SARD ZP RM 2E661 103 ARMY PENTAGON WASHINGTON DC 20310-0103
1	ASST SECY ARMY RESEARCH DEVELOPMENT ACQUISITION SARD ZS RM 3E448 103 ARMY PENTAGON WASHINGTON DC 20310-0103
1	ASST SECY ARMY RESEARCH DEVELOPMENT ACQUISITION SARD ZT RM 3E374 103 ARMY PENTAGON WASHINGTON DC 20310-0103
1	UNDER SEC OF THE ARMY DUSA OR RM 2E660 102 ARMY PENTAGON WASHINGTON DC 20310-0102
1	ASST DEP CHIEF OF STAFF OPERATIONS AND PLANS DAMO FDZ RM 3A522 460 ARMY PENTAGON WASHINGTON DC 20310-0460
1	DEPUTY CHIEF OF STAFF OPERATIONS AND PLANS DAMO SW RM 3C630 400 ARMY PENTAGON WASHINGTON DC 20310-0400

NO. OF COPIES	ORGANIZATION
1	ARMY RESEARCH LABORATORY AMSRL SL PROGRAMS AND PLANS MGR WSMR NM 88002-5513
1	ARMY RESEARCH LABORATORY AMSRL SL E MR MARES WSMR NM 88002-5513
	ABERDEEN PROVING GROUND
1	CDR USATECOM AMSTE-TA
2	DIR USAMSAA AMXSY-ST AMXSY-D
4	DIR USARL AMSRL-SL, J WADE (433) M STARKS (433) AMSRL-SL-C, J BEILFUSS (E3331) AMSRL-SL-B, P DEITZ (328)

NO. OF COPIES	ORGANIZATION
1	COMMANDER NAVAL SURFACE WARFARE CTR CODE G29 T WASMUND DAHLGREN DIVISION DAHLGREN VA 22448-5000
1	ASC/XREWA DR K MCARDLE EGLIN AIR FORCE BASE FL 32542-5600
1	DIRECTOR PATRIOT PEO SFAE MD PAO SE W GILCHRIST PO BOX 1500 HUNTSVILLE AL 35807
1	DIRECTOR CORPS SAM SFAE MD SM E HS G PRESTON PO BOX 1500 HUNTSVILLE AL 35807
1	DIRECTOR THE JOHN HOPKINS UNIVERSITY APPLIED PHYSICS LABORATORY A EATON ATM PANEL CHAIRMAN LAUREL MD 20723-6099

NO. OF COPIES	ORGANIZATION
	ABERDEEN PROVING GROUND
1	CDR USAMSAA AMXSY-D, R. SMITH
25	DIR USARL AMSRL-SL-B W WINNER AMSRL-SL-BA M VOGEL A KIWAN J MORRISSEY R BOWERS S POLYAK D TEN BROECK W THOMPSON R WALTHER J FRIES K KIM E WEAVER L ROACH AMSRL-SL-BL M RITONDO J HUNT R DIBELKA S JUARASCIO E DAVISSON O LITT AMSRL-SL-BS R GROTE D BELY AMSRL-SL-BV L MOSS R SHNIDMAN J POLESNE R SAUCIER
3	DIR EAC W HUGHES EAC-SV, D HASKELL EAC-AD, R REDWINSKI

REPORT DOCUMENTATION PAGE

Form Approved
OMB No. 0704-0188

1. AGENCY USE ONLY *(Leave blank)*	2. REPORT DATE	3. REPORT TYPE AND DATES COVERED
	August 1997	Final, Mar 96 - Mar 97

4. TITLE AND SUBTITLE
An Overview of High-Explosive (HE) Blast Damage Mechanism and Vulnerability Methods

5. FUNDING NUMBERS
PR: 1L162618AH80

6. AUTHOR(S)
Abdul R. Kiwan

7. PERFORMING ORGANIZATION NAME(S) AND ADDRESS(ES)
U.S. Army Research Laboratory
ATTN: AMSRL-SL-BA
Aberdeen Proving Ground, MD 21005-5068

8. PERFORMING ORGANIZATION REPORT NUMBER
ARL-TR-1468

9. SPONSORING/MONITORING AGENCY NAMES(S) AND ADDRESS(ES)

10.SPONSORING/MONITORING AGENCY REPORT NUMBER

11. SUPPLEMENTARY NOTES

12a. DISTRIBUTION/AVAILABILITY STATEMENT
Approved for public release; distribution is unlimited.

12b. DISTRIBUTION CODE

13. ABSTRACT *(Maximum 200 words)*

An overview of high-explosive (HE) blast phenomenology, its models, methods, and the scaling of results are presented. Experimental data of HE blast damage to various types of structures are also presented, together with some of the HE blast structural damage models. Empirical vulnerability models of weapon systems to HE blast are also discussed.

14. SUBJECT TERMS
high explosive, blast, structures, structural damage, damage mechanisms, damage models, scaling methods, vulnerability methods, lethal blast kill radius, blast contours

15. NUMBER OF PAGES
54

16. PRICE CODE

17. SECURITY CLASSIFICATION OF REPORT	18. SECURITY CLASSIFICATION OF THIS PAGE	19. SECURITY CLASSIFICATION OF ABSTRACT	20. LIMITATION OF ABSTRACT
UNCLASSIFIED	UNCLASSIFIED	UNCLASSIFIED	UL

INTENTIONALLY LEFT BLANK.

USER EVALUATION SHEET/CHANGE OF ADDRESS

This Laboratory undertakes a continuing effort to improve the quality of the reports it publishes. Your comments/answers to the items/questions below will aid us in our efforts.

1. ARL Report Number/Author ARL-TR-1468 (Kiwan) Date of Report August 1997

2. Date Report Received _____

3. Does this report satisfy a need? (Comment on purpose, related project, or other area of interest for which the report will be used.) _____

4. Specifically, how is the report being used? (Information source, design data, procedure, source of ideas, etc.) _____

5. Has the information in this report led to any quantitative savings as far as man-hours or dollars saved, operating costs avoided, or efficiencies achieved, etc? If so, please elaborate. _____

6. General Comments. What do you think should be changed to improve future reports? (Indicate changes to organization, technical content, format, etc.) _____

CURRENT ADDRESS

Organization

Name E-mail Name

Street or P.O. Box No.

City, State, Zip Code

7. If indicating a Change of Address or Address Correction, please provide the Current or Correct address above and the Old or Incorrect address below.

OLD ADDRESS

Organization

Name

Street or P.O. Box No.

City, State, Zip Code

(Remove this sheet, fold as indicated, tape closed, and mail.)

(DO NOT STAPLE)

DEPARTMENT OF THE ARMY

OFFICIAL BUSINESS

NO POSTAGE
NECESSARY
IF MAILED
IN THE
UNITED STATES

BUSINESS REPLY MAIL
FIRST CLASS PERMIT NO 0001,APG,MD

POSTAGE WILL BE PAID BY ADDRESSEE

DIRECTOR
US ARMY RESEARCH LABORATORY
ATTN AMSRL SL BA
ABERDEEN PROVING GROUND MD 21005-5068